Hybrid Advances 5 (2024) 100125

Contents lists available at ScienceDirect

Hybrid Advances

journal homepage: www.journals.elsevier.com/hybrid-advances

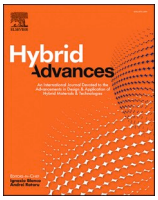

Cavitation resistance of FeMnCrSi coatings processed by different thermal spray processes

Rodolpho F. Vaz [a], Luciana L. Silveira [b], Juliane R. Cruz [c,*,1], Anderson G.M. Pukasiewicz [b]

[a] Thermal Spray Centre (CPT), University of Barcelona, Dpt. CMiQF, Carrer de Marti i Franques 1, 08028, Barcelona, Spain
[b] Federal University of Technology Parana (UTFPR). R. Doutor Washington Subtil Chueire, 330, Jardim Carvalho, 84017-220, Ponta Grossa, PR, Brazil
[c] Center of Thermal Spray Research (CTSR). State University of New York at Stony Brook. Room No. 130, Heavy Engineering Building, Stony Brook, NY, 11794-2275, USA

ARTICLE INFO

Keywords:
FeMnCrSi
Cavitation
Coating
Thermal spraying
Cladding
Wear

ABSTRACT

Cavitation-resistant FeMnCrSi coatings were developed in the past years as a cost-effective alternative to Co-containing alloys to increase the lifespan of hydraulic machinery. The effect of different chemical compositions, surface finishing, and post-processing treatments was investigated for various processing techniques, namely: Arc Spraying Process (ASP), High-Velocity Oxy-Fuel (HVOF), High-Velocity Air-Fuel (HVAF), Plasma Transferred Arc (PTA), and Cold Gas Spray (CGS). This works consists of a compilation and review of original and literature results, and discusses the microstructure changes imparted by each type of processing and their impact on the coating properties and cavitation resistance. Low heat input high-velocity processes (HVOF, HVAF, CGS) developed a reduced degree of oxidation and porosity, accounting for a cavitation resistance higher than that of the coatings that ASP processed. In addition, ASP coatings showed reduced cohesive strength, with the oxidized inter-splat interface being a preferential site for crack propagation.

1. Introduction

Water flow is one of the earliest forms of renewable energy, long used for irrigation since the development of agriculture in Mesopotamia in 6000 BCE [1]. Its motion is also being used for producing clean electricity, which currently accounts for 16 % of all electricity generation worldwide [2,3]. In Brazil, 70 % of the electricity generated comes from hydropower plants [4], while in Canada, this percentage is currently about 61 % [5]. China works toward increasing hydroelectric energy production. There, the number of installed hydropower plants increased more than four times since 2000 [6]. Japan has plans to improve the use of small and medium hydropower plants in its energy generation matrix by 11 % [7]. Despite various configurations available for the different types of hydropower plants, the principle of operation remains the same: converting the water flow into mechanical energy (by the rotation of an axle) and then converting this rotation into electricity by an electricity generator.

An essential component for hydropower plants is/are the runner/runners, also known as hydro turbines. The selection of the most efficient runner depends on the characteristics and configuration of the power plant, mainly on the site's features, available head, and the river's flow regime [8–10]. The ASTM A743 grade CA6NM martensitic stainless steel has advantages over low carbon and austenitic stainless steel to manufacture runners. It includes a higher mechanical resistance, fatigue life, and toughness. New large CA6NM runners are produced by welding, making them susceptible to adverse microstructural changes, reducing the material fracture toughness, mainly if post-welding heat treatments are not adequately performed [11–16].

Wear in runners is a common problem in hydropower plants. One type of wear is the erosion of its components, which results from the impingement of solid particles on the material, resulting in mass loss, hydraulic profiles changing, consequently, equipment efficiency reduction [13]. Erosive particle properties, runner's material properties, and equipment operating conditions can affect the wear of turbines [17]. The deposition of erosion-resistant coatings by thermal spray processes has been widely used to minimize erosion wear [17–20].

* Corresponding author.
E-mail addresses: rvaz@cptub.eu (R.F. Vaz), luciana.llsilveira@gmail.com (L.L. Silveira), juliane.rcruz@gmail.com (J.R. Cruz), anderson@utfpr.edu.br (A.G.M. Pukasiewicz).
[1] (Present address) Graduate Program in Mechanical Engineering (PGMec), Federal University of Parana (UFPR), Av. Cel. Francisco H. dos Santos, 230, Jardim das Americas, 81530-000, Curitiba, PR, Brazil.

https://doi.org/10.1016/j.hybadv.2023.100125
Received 12 September 2023; Received in revised form 1 December 2023; Accepted 4 December 2023
Available online 13 December 2023

The cavitation phenomenon is another important wear issue affecting runners' integrity. According to literature, the cavitation phenomena is related to the change in velocity and pressure fields in a liquid flow, accounting for the creation of microbubbles when the vapor pressure is reduced and their implosion when the vapor pressure is reestablished [21–23]. This implosion generates microjets of fluid that reach the material surface with enough energy to erode the hydraulic component by a fatigue mechanism [24,25]. Therefore, special coatings have been applied by welding and thermal spray processes to improve the cavitation resistance, notably the deposition of stainless steels containing high fractions of Co [26–30] processed by the GMAW process (Gas Metal Arc Welding) [31–33]. Different works calculated the maximum pressures induced by the bubbles implosion, p_{max}, calculated from single collapsing bubbles using an ultrasonic vibratory apparatus observed values between 2400 and 3500 MPa using copper [34]. Meanwhile some simulations indicated peak pressures from 1400 to 2900 MPa in Al7075 alloy independent on the flow pressure or velocity of cavitating fluid [35]. In another study, the impact pressure micro-jet produced by in ultrasonic cavitation occurs in a range near 1000–1200 MPa [36]. In this case the cavitation peening load can directly affect the magnitude of compressive residual stress observed in the material subjected to cavitation wear [37]. The strain phase transformation γ→ε and γ→α' in steels occurs during the plastic deformation in values between 1000 and 2000 MPa, depending on the chemical composition of the material [38–40]. However, it is well known that γ→ε transformation can occur at significantly lower stresses, depending on the stacking-fault energy (SFE).

The mechanism of the strain-induced nucleation was firstly studied by Olson and Cohen in 1972 [41]. In this work they observed that ε-martensite can form in austenite phase when the stacking-fault energy (SFE) is very low. The nucleation sites and α′ embryos are generated by two intersecting shear systems in the austenite along {111} and <112>. Bogachev and Mints developed the first studies that observed that metastable austenite has the capacity to raise substantially the resistance of the surface of a material against dynamic loads observed in different kinds of mechanical wear. According to Schastlivtsev and Filipov, Bogachev and Mints suggested that low- and medium-carbon austenite steels containing Fe, Mn, Cr and C steels presents high cavitation and erosion resistance due to the low energy transformartion from austenite to martensite under loading [42]. Different FeMnCrSi alloys have been developed and studied in the last decade as a lower-cost alternative for runners' erosion-resistant coatings [29–33,43]. Similar to the stainless steels with Co and other FeMn-based alloys, the FeMnCrSi alloys have low SFE and the ability to develop strain-induced martensitic transformations [29,44], which promote strain hardening and superior cavitation resistance [44,45]. These alloys constitute a class of Advanced High-Strength Steels (AHSS), with the presence of transformation-induced plasticity steels and twinning-induced plasticity steels [46]. Different FeMnCrSi chemical compositions were evaluated, varying the content of B, Ni, N, and other alloying elements to achieve the highest possible cavitation resistance.

Nowadays, the development of green materials, with better sustainability processes and lower impact on nature and human health, is one of the main objectives of metallurgists and materials engineers. Ni is an essential element for human body functionality. However, different health problems: include cardiovascular problems, lung fibrosis, carcinogenic and teratogenic potential, and allergic issues associated with high Ni presence [47]. The replacement of the Ni by Mn in food contact stainless steel showed a low safety risk because there is not migration of Mn from stainless steel to the food [48].

This work aims to compile the available literature on the cavitation resistance of FeMnCrSi coatings processed by different thermal spray processes, i.e., High-Velocity Oxy-Fuel (HVOF), High-Velocity Air-Fuel (HVAF), Arc-Spray Process (ASP), Cold Gas Spray (CGS), and Plasma Transferred Arc (PTA). In addition, the effect of post-processing treatments, such as shot-peening, remelting, and cold working is also discussed in terms of microstructure and mechanical properties changes, distilling trends expected of FeMnCrSi coatings for a wide range of processing conditions.

2. Development of the FeMnCrSi alloys

In abrasion and erosion wear, surface properties such as hardness and friction coefficient dictate the wear damage rate and the material wear resistance [49,50]. However, for cavitation, the mechanical fatigue resistance has been extensively correlated to its cavitation resistance [48,51,52]. Moreover, a crucial factor is the material capacity for absorbing energy from the cavitation shockwaves, achieved by strain-induced metallurgical transformations. Different microstructural responses can be triggered under cavitation, including dislocation motion, Twinning-Induced Plasticity (TWIP), and Transformation-Induced Plasticity (TRIP) [53]. These findings have developed several cavitation-resistant materials, such as stainless steel, shape-memory materials, Co-based alloys, Ni–Al intermetallic compounds, and TiC-reinforced composites, among others [54–62].

Typically, metallic alloys are not thermodynamically stable, retaining crystallographic imperfections or defects. The arrangement and density of these defects, such as dislocations, grain boundaries, porosity, and inclusions, have been frequently presented in the literature. Still, less attention has been placed on the role of bulk and localized variation of chemical composition in the material or partitioning effects on phase metastability. For example, some alloys have presented TRIP and TWIP [63], which are mechanisms seen in Metastable Austenite (MSA) steels, studied since the '60s. This mechanism was the starting point for developing wear resistant FeMn alloys [41,42].

Different FeCrMnSi alloys started as a variation of high alloy stainless steel with the main goal of reducing the SFE by adding certain elements, promoting the formation of twin or ε-martensite during deformation, and increasing the capability of energy absorption before fracture. The phenomenon of cavitation-induced martensitic transformation improves the cavitation resistance of FeCrMnSi coatings. Low SFE materials show a Face-Centered Cubic (FCC) structure, which transforms into the ε-martensite Hexagonal Closed-Packed (HCP) structure with the deformation [62,64–66]. These martensitic transformations in Cr–Mn steels develop according to the path γ→ε→α′. However the transformation γ→ε is initiated in small degrees of deformation, ε→α′, as well as γ→α' occurs at high degrees [67]. The study of a manganese-free deposited coating of the Fe–Cr–C–Al–Ti type with the structure of MSA also showed that γ→α′ transformation takes place after cavitation [65]. Fe–10Cr–10Ni-xC also show an incubation period inversely proportional with the carbon concentration, which correlated very well with the Critical Strain Energy. In these alloys, the transformation from the austenite phase to the martensite phase was observed, confirming that the cavitation energy was absorbed into the matrix and improved the cavitation erosion resistance [68,69]. The alloy Fe–20Cr-1.7C-1.0Si also showed a strain induced phase transformation and demonstrate a higher cavitation resistance due to energy absorption due martensitic transformation [70]. It was evidenced that FeMnCrSi alloys with low SFE exhibit TRIP martensitic transformation, increasing the work hardening rate [71–74]. FeMnCrSi alloys presented in this work have been formulated to guarantee good mechanical properties and an SFE mathematically low enough to allow the TRIP phenomena, which is possible for stacking fault energies under 16 mJ/m^2 [71,74], that correspond to Fe-based alloys with less than 0.2 wt%C and approximately 15–20 wt%Mn, 8–11 wt%Cr, and 4–6 wt%Si. Other chemical composition can be produced adding other alloying elements to the FeMnCrSi alloys with the objective to alter their performance under the cavitation loading.

The research conducted by Lang et al. [75] observed a reduction of the SFE in high Mn Fe–C–Mn–Cr steel with Cr content increase, and this behavior is independent of Mn and C contents. On the other hand, Si reduced the SFE only in alloys with higher Mn content. The Fe–15Mn-0.6C–6Cr–3Si alloy showed higher tensile strength due to high

negative values of $\Delta G\gamma\rightarrow\varepsilon$ and low SFE. According to Blinov et al. [76], adding between 10 and 15 wt% of Mn changed the martensitic transformation $\gamma\rightarrow\alpha$' to $\gamma\rightarrow\varepsilon$. More than 15 wt% of Mn promoted only $\gamma\rightarrow\varepsilon$ transformation, which was suppressed in alloys with high Mn content (25–35 wt%). It is also commented that the effect of Cr addition on the $\gamma\rightarrow\varepsilon$ transformation was different in Ni and Mn austenite alloys. It occurs because the Cr content in the Cr–Ni alloy was below the solubility limit, while in the Cr–Mn alloys, the Cr amount was near the solubility limit.

The chemical composition of different alloys and the findings observed in the literature are summarized in Table 1. The wide variety of chemical compositions makes it challenging to compare the various alloys and the exact influence of each alloying element. However, some important aspects can be defined: (i) lower SFE correlates with the formation of ε-martensite; (ii) whether α or ε-martensite formation is desired will depend on the wear process, e.g., sliding or cavitation, with ε-martensite formation improving cavitation resistance and α-martensite showing better performance against sliding wear; (iii) work hardening is an essential aspect of the strain-induced phase transformation; (iv) the presence of precipitates, depending on their type, volume fraction, coherency, and distribution, among other properties, induces significant improvements in the tensile and cavitation resistance.

3. Influence of the feedstock features

Each deposition process for FeMnCrSi coatings needs some feedstock characteristics, e.g., format of powder or wire. This last one is used for the ASP process, in which the wires must be conductors to allow electrical contact between the cathode and the anode in the gun. The wire may be solid or metal-cored, consisting of a metallic outer strip filled with flux or metal powder whose mixture determines the final chemical composition. Metal-cored wires with hard particles have also been used as a convenient way to produce Fe-based cermet coatings. Examples of such wires include Cr_7C_3, Cr_3C_2, and WC carbides inside a carbon steel strip and FeCrN/CBN inside a 304 stainless steel strip, among many others [81–87]. For the FeMnCrSi alloys, an AISI 301 stainless steel was used as the strip, and the filler powders amount and composition (Fe, Mn, Fe–Cr–N, Fe–Mn, Fe–Si, Fe–Si–Mn, and Fe–B) were selected and mixed to adjust the final designed wire composition [88].

The wire size or diameter influences the ASP optimal parameters (voltage and current) and the size of the distribution of the droplets in the plume. It results in different particles' velocity and energy, and coating microstructure, phases, metallic particles, oxide layers, pre-solidified particles, and porosity, influencing the coating performance [81,88,89]. For the Fe-based alloy Fe–25Cr–21WVMnSi, wires with a diameter of 2.4 mm instead of 1.6 mm promoted thicker metallic lamellae, higher porosity and adhesion, but lower micro-hardness and abrasive resistance [90]. This behavior is an example of the feedstock influences on the microstructure and mechanical properties of the ASP coatings.

Different techniques can be used to produce alloy feedstock powders. A method is the mixture of elemental powders and/or pre-alloyed powders by milling, resulting in a fine homogeneous mixture of powders. In contrast, the inert gas atomizing process produces high sphericity powders with controlled chemical composition and particle size distribution. Inert gas atomization process technique is significantly more expensive than milling, not yet as widely available, and can get even more expensive. In contrast, water atomization is cheaper and produces an irregular powder shape with higher oxidation [91–93]. For arc melting processes, like PTA, such differences (water and inert gas atomization) are not expected to promote a severe influence [94]. However, high-velocity thermal spraying can affect the final coating morphology and, consequently, the coating performance [95–98].

As seen in Fig. 1, ASP processing led to a loss of Mn and Si and, in some cases, Cr, accounting for a relative increase in the fraction of Ni left in the coating. Significant loss of Si occurred in PTA processing using a

Table 1
Development of different FeMnCrSi alloys.

Year	Ref.	Materials	Findings
'50s	[42]	Fe–Mn–Cr–C	The first work presenting a new application of MSA, i.e., the material capacity to have an improved surface response under dynamic contact loads on wear
1972	[42]	Fe–Ni–Cr	This work introduces and explains the terms "strain-assisted martensite" and "strain-induced martensite". The work also shows the relationship between stress and martensite appearance temperature.
1997	[30]	Fe–14Mn–0.6Si–17Cr	The superior cavitation resistance is mainly attributed to the alloy's high work-hardening ability.
2000	[33]	Fe–14/18Mn–6Si–8Cr–6Ni	FeMnSiCrNi SME is expected to have the lowest SFE among the FeMnCrSi alloys.
2003	[29]	Fe–25Mn–6Si–7Cr–Cu; Fe–21Mn–6Si–9Cr–Cu	Phase transformation influences the cavitation resistance of steels. TRIP improves wear resistance.
2004	[29]	Fe–21Mn–6Si–9Cr	ε-martensite plays a key role in the contribution of the cavitation erosion resistance of the FeMnSiCr.
2004	[74]	Fe–22Mn-0.6C	SFE<18 mJ mol^{-1}, the ε-martensitic transformation occurs, while for 12 mJ mol^{-1}<SFE < 35 mJ mol^{-1} mechanical twinning takes place.
2005	[77]	Fe–C–Ti–C–B	Heat treatment of welded FeCTiCB alloy ensures the structure of MSA in the metallic matrix and high resistance to abrasive wear.
2006	[57]	Fe–20Cr–15Mn–1.0Si	Additions of Mn exceeding 10 wt % improves the cavitation erosion resistance of the Fe-based alloy. The improvement is likely due to the development of the $\gamma\rightarrow\varepsilon$ strain-induced martensitic transformation.
2013	[73]	Fe–5/10Mn–0/10Ni–12Cr	Cavitation resistance improves with the Mn content, while the Ni addition reduces the Fe-based alloys wear resistance.
2015	[78]	Fe–8/16Cr–5Mn	Strength and fracture strain are more important factors for determining the cavitation erosion resistance than the volume fraction of transformed α-martensite.
2016	[72]	Fe–12Cr–5/20Mn	Specifically, the wear resistance of alloys undergoing $\gamma\rightarrow\varepsilon$ transformation in higher compared to those undergoing the $\gamma\rightarrow\alpha'$ transformation. This is attributed to the higher hardness of α'-martensite.
2019	[79]	Fe–18Cr–16Mn–4Si–B	Boron affects the erosion mechanisms of coatings, accounting for a reduction in maximum erosion rates.
2020	[80]	Fe–12Mn–2Cr–3Ni–0.3B	Presence of M_2B-type borides and strain-induced transformation causes a significant enhancement of the tensile properties.
2021	[75]	Fe–15Mn–0/3Si–4/6Cr	Changes in the Fe-based alloy chemical composition results in higher tensile strength and lower SFE, promoting the ε-martensitic transformation under stress.

(*continued on next page*)

Table 1 (*continued*)

Year	Ref.	Materials	Findings
2021	[69]	Fe–8Cr–1.5Al–1.0Ti–0.6C	Changes in Fe-based chemical composition increases martensite content before cavitation from 29.5 to 73.5 %.

mixture of elemental and pre-alloyed powders as feedstock. On the other hand, in coatings processed by PTA using atomized powders, Si loss was suppressed. In coatings processed by HVOF, chemical composition fluctuations are subtler, with a slight decrease in Si and Ni content, accounting for a relative increase in the fraction of Mn and Cr in the coatings.

In FeMnCrSi alloys, some elements are more oxygen-sensitive than others, mainly Si and Mn, as predictable from Ellingham diagrams [81]. The reduction of these elements is relevant for the performance of FeMnCrSi coatings because the chemical composition was designed to obtain a desired low SFE [73,74], which is crucial for the evolution of strain-induced staking fault as an energy absorption mechanism to improve the coating cavitation resistance.

The most significant chemical composition variations occurred for PTA processing using mechanical mixtures of powders and ASP using metal-cored wire feedstock, composed of an AISI 301 stainless steel strip filled with a mixture of elemental and pre-mixed powders (Fe, Mn, Fe–Cr–N, Fe–Mn, Fe–Si, Fe–Si–Mn, and Fe–B) [87]. Pre-mixed and elemental powders are more readily available to react with oxygen during ASP deposition. Different from the atomized powders, elements in solid solution may require higher activation energies to break the pre-existing chemical bonds, allowing for subsequent reaction with oxygen.

In ASP processing, oxidizing reactions occur on the heat source (zone of an electric arc), during in-flight travel, and in the solidification of lamellae [99–102]. Nevertheless, the first one causes the most significant chemical decompositions for ASP, as confirmed by the greater variation in chemical composition from the wire to the particle and less variation from the particle to lamellae [88].

Previous studies indicated that Ni and B addition in wear-resistant MSA Fe-based alloys [77,103–105] reduced the oxidation, preventing unwanted chemical decomposition and improving the coatings mechanical resistance. In FeMnCrSi coatings processed by ASP, the addition of 1.0 wt% B promoted a reduction in oxide content from 10.5 % to 4 % and an increased hardness from 350 to 500 HV, maintaining the porosity levels at about 1.5 % and the adhesion strength between 30 and 35 MPa [87]. In coatings processed by HVOF, Ni additions reduced the oxide content and porosity of the coatings, while B additions improved the hardness of the coatings [106]. In coating processed by PTA, progressive B addition up to 1 wt% led to grain refinement with the formation of a eutectic phase composed of austenite and FeCrB phase, and a progressive increase in hardness. The formation of FeCrB phase reduced the content of Cr in solid solution from about 19 to 15 wt%, which could increase the SFE [79].

Despite the melting and solidifying process that occurred during PTA deposition, the elemental powder mixture processing presents higher oxidation with an important change in the chemical composition of the deposited alloy. For example, in work conducted by da Cruz et al. [79], the alloys produced with this route showed a significant Si reduction in solid solution because of silicon oxide formation. This behavior was not observed during the processing of atomized alloys. Similar behavior was observed on the FeMnCrSi alloys deposited with metal-cored wire. In this study, Vaz et al. [88] observed the reduction of the Mn, Cr, and Si elements because of oxides formation or their vaporization. Therefore, the stability of the chemical composition, from feedstock to coating, will be directly affected by the materials processing, where the selective oxidation process during a deposition must be compensated when the alloy is processed by elemental powder mixture.

4. Microstructure of FeMnCrSi coatings processed by different thermally spraying processes

4.1. Factors affecting the coatings porosity and oxide content

The microstructures of FeMnCrSi coating processed by different spraying methods are shown in Fig. 2, which consists of optical microscopy images under low and high magnification. Metallic thermally sprayed coatings are typically composed of distinct phases, including metallic phases, oxide layers, pores, and pre-solidified droplets or particles. Despite the similar chemical compositions, Fig. 2 shows that the microstructure of the coatings differs from one another in terms of oxide content, porosity content, and degree of particle melting/flattening, among others.

EDS chemical composition mapping of FeMnCrSiB coatings processed by HVOF and PTA are shown in Figs. 3 and 4, respectively. Results illustrate how the oxidizing atmosphere of HVOF processing leads to higher degrees of oxidations in comparison to coatings processed by PTA under flowing inert gas atmosphere.

A summary of these microstructural features for FeMnCrSi coatings, processed by different spray techniques, is presented in Fig. 5. In Fig. 5a, it is possible to see that higher porosity levels were observed in coatings processed by ASP. For higher kinetic energy thermal spray processes, the FeMnCrSi alloys presented denser coatings, as seen in Fig. 5b,c,d. In these coatings, the higher velocity of the particles is converted into

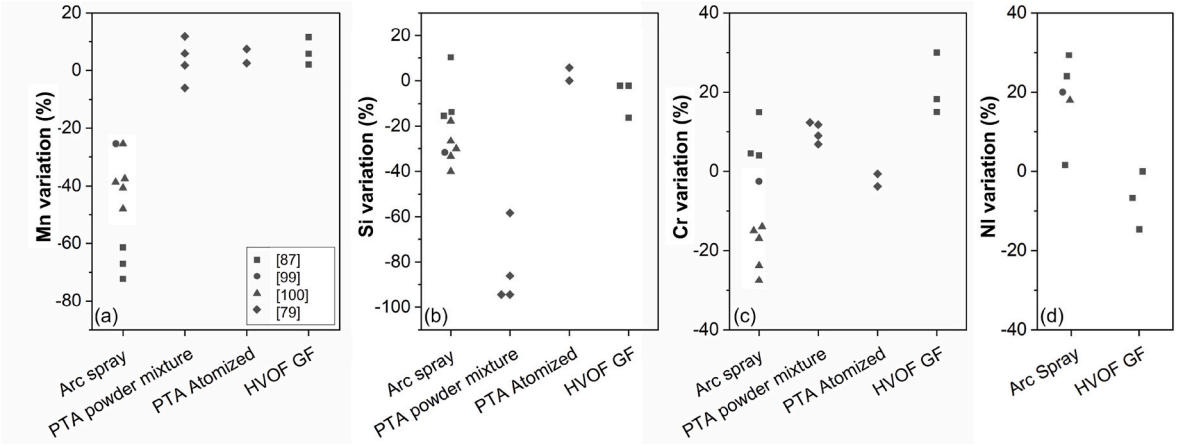

Fig. 1. Chemical composition changes during the processing of FeMnCrSi(Ni)(B) coatings by different processes, showing fluctuations in the content of (a) Mn, (b) Si, (c) Cr, and (d) Ni.

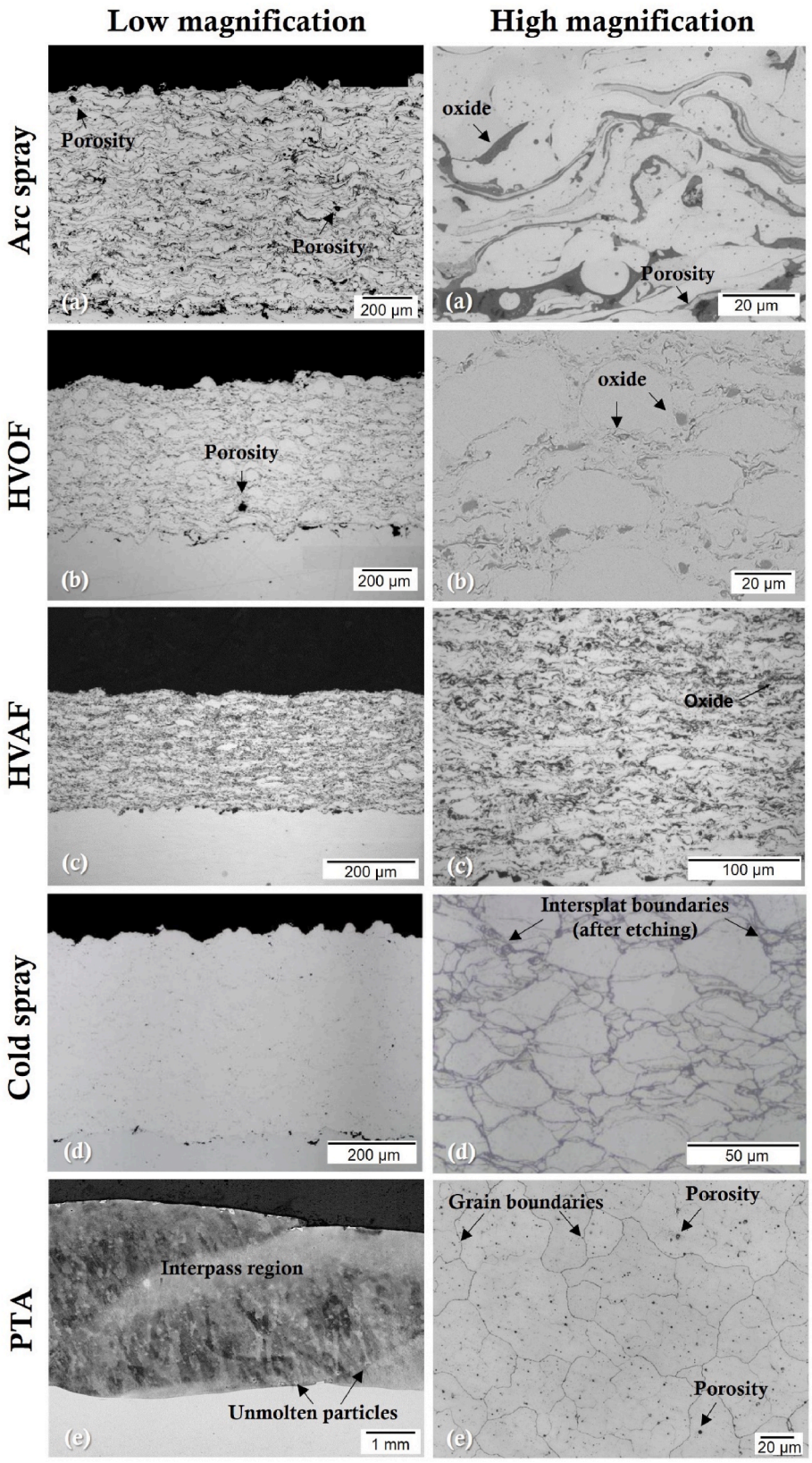

Fig. 2. Microscopic aspect of FeMnCrSi(Ni) coatings processed by (a) ASP, (b) HVOF, (c) HVAF, (d) CGS, and (e) PTA. A high degree of particle flattening in coatings processed by ASP is associated with higher heat input. The reduced degree of porosity in coatings processed by high-velocity processes (HVOF, HVAF, and CGS). A lower degree of flattening in coatings processed by CGS is associated with the reduced processing temperature and, consequently, higher yield strength. Microstructure of PTA coatings showing fully molten and recrystallized grains [50,79,87,107,108].

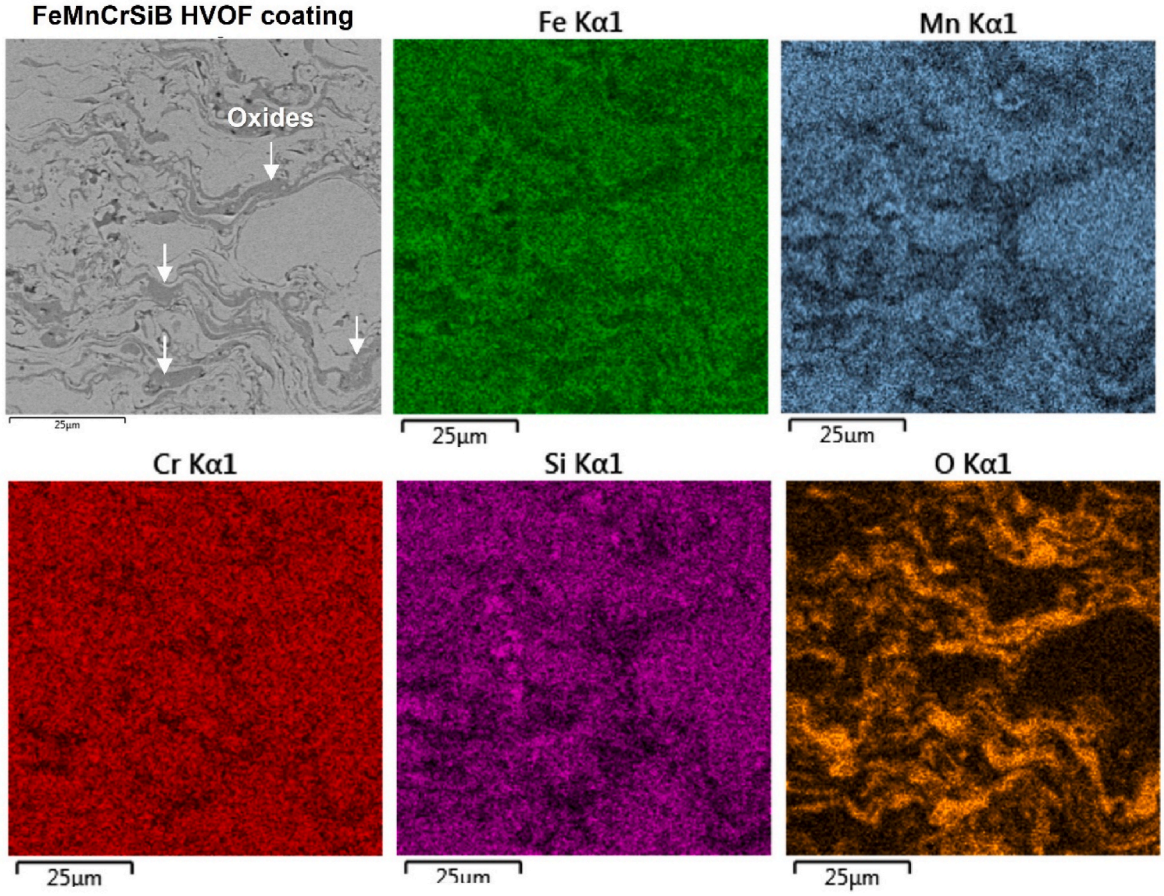

Fig. 3. EDS chemical composition map of FeMnCrSiB coating processed by HVOF showing high content of oxides in the intersplat region.

particle deformation and coating densification. As a result, fine and homogeneously distributed micro porosities are seen in coatings processed by PTA ranging from 0.2 to about 0.8 wt%.

The following discussion considers the role of heat input, thermal and kinetic energy, and particle size on the properties of the FeMnCrSi coatings.

HVOF-kerosene fuel was found to geneate denser FeMnCrSi coatings than HVOF-propylene fuel coatings. Higher particle velocities are achieved by processing with liquid fuel (up to 1012 m s^{-1}) with similar particle temperatures, about 2050 °C in all experiments, which was close to the values observed during HVOF-propylene and ASP processing of FeMnCrSi and CaviTec alloys (Fe-based 10 wt%Co) [25,87]. The higher velocities of the HVOF-kerosene fuel sprayed particles increase the kinetic energy and produced dense coatings [108]. Similar to what was observed in coatings processed by ASP [87], in FeMnCrSi coatings processed by HVOF, the statistical analysis for the parameters selection showed a direct correlation between the porosity and the standoff distance, as well as an inverse correlation with the powder feed rate [106].

The porosity content of ASP FeMnCrSi coatings increases with spray distance [110]. With the increase in the spray distance, a possible reduction in the particle temperature and velocity could reduce the flattening rate. Nevertheless, such porosity values are still quite low when compared to those expected for ductile material processed by electric arc spray, expected to range from 8 to 15 % [83]. Another factor contributing to a higher degree of porosity in coatings processed by ASP is the heterogeneity of lamellae size due to a broad sprayed particle size distribution. The heterogeneity of lamellae size occurs because the melting of the feedstock wires followed by the compressed air atomization produces much larger droplets at the anode wire (positive polarity) than at the cathode wire (negative polarity) [111,112]. The average particle velocities were about 105–125 m s^{-1} [87], in the lower range within the different spraying processes.

As a result, the higher dwell time in-flight could increase the degree of particle oxidation. On the other hand, this is balanced, to some extent, by the relatively high average particle diameter (d50 in the order of 57–67 µm), leading to a reduced surface area available for oxidation. In a variation of this process, the High-Velocity Arc-Spraying (HVAS) process, equipment modifications (especially in the gun) were shown to increase particles velocity, resulting in a kinetic energy increase of 40 % [113], improving particle flattening and cohesion. Using the HVAF, the adhesion strength of around 30 MPa was obtained for FeCrNi/CBN coatings [81], and a predominantly amorphous Fe-based phase was obtained with adhesion higher than that produced by HVOF [86]. Nevertheless, despite the lower particle velocities of the process, the adhesion strength of FeMnCrSi coatings processed by ASP was higher than 30 MPa, with similar performance to some HVOF coatings. For the FeMnCrSi alloys, cold spray processing resulted in a shallow porosity content, below 1 %, low oxide content as seen in the top Fig. 2d, and no phase transformation during the deposition, keeping the same γ-austenite from the initial powder condition. Similar characteristics were obtained for the samples sprayed with N_2 at 1000 °C and He at 600 °C.

Despite the higher velocity and lower dwell times, FeMnCrSi coatings processed by HVOF presented a similar degree of oxidation as the ASP coatings. One factor contributing to this relatively high oxide content is the smaller particle size of the feedstock used in the HVOF depositions, with d50 ranging from 32 to 36 µm, nearly half those used in ASP processing, resulting in a larger surface area for oxidation [87]. A study on the selection of HVOF FeMnCrSi particle size distribution showed that particle size ranges below 45 µm resulted in the lowest

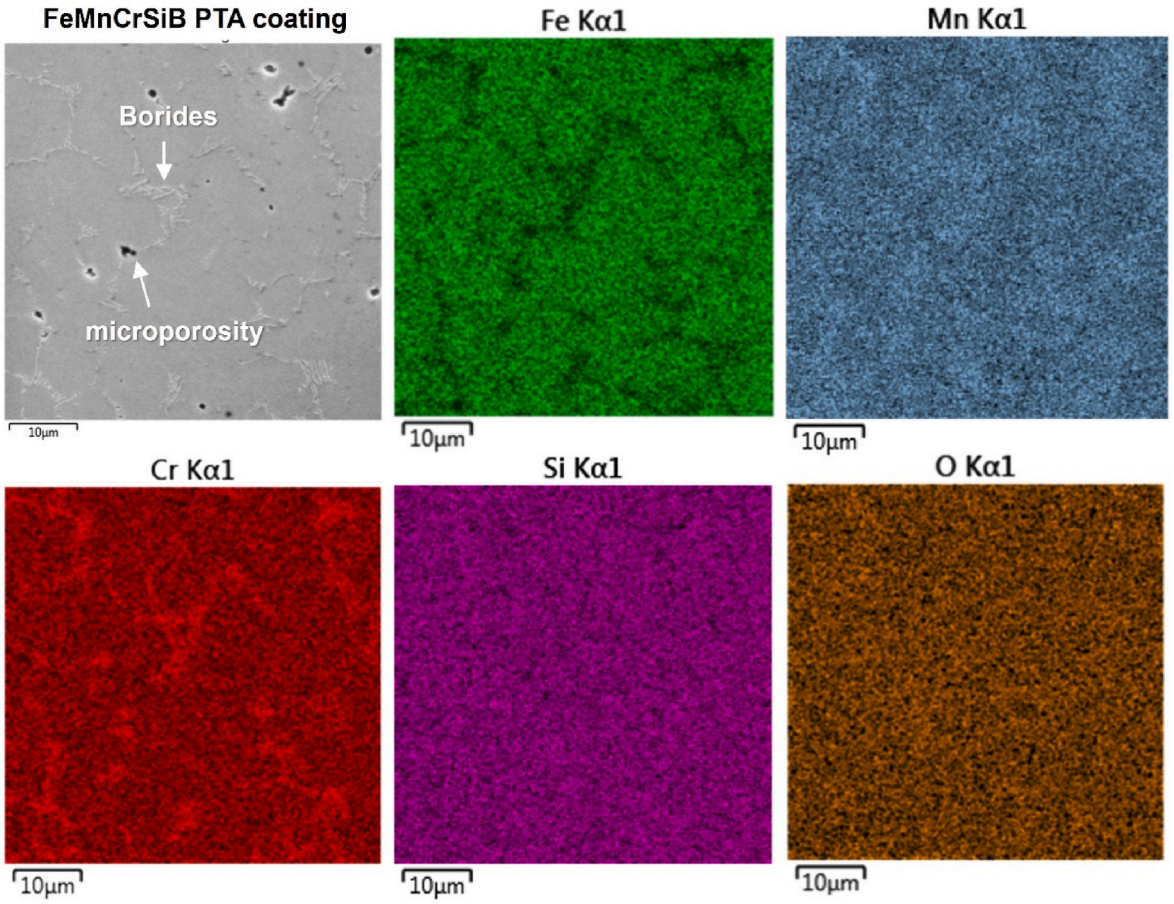

Fig. 4. EDS chemical composition map of FeMnCrSiB coating processed by PTA showing no significant oxide formation, but Cr-rich borides formation in the interdendritic region.

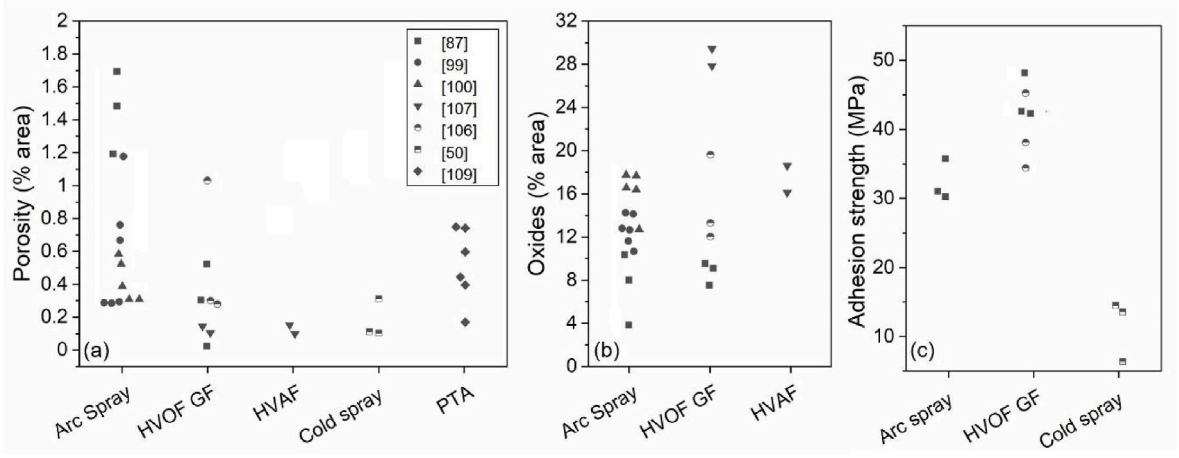

Fig. 5. (a) Porosity content, (b) oxide content and (c) adhesion strength of FeMnCrSi(Ni) coatings processed by different processes. Lower porosity levels are achieved with high-velocity processing (HVOF, HVAF, and CGS). Compared to arc spray, a relatively high degree of oxidation in coatings processed by HVOF GF and HVAF could be associated with the smaller particle size cut and, consequently, the higher surface area available for oxidation. The superior adhesion strength of coatings processed under higher heat inputs (HVOF and ASP), in comparison to CGS.

porosity levels (about 0.04 %). In contrast, the one in the −63 + 45 µm range presented the lowest oxide content (about 4.85 %) well distributed in the coating but, with a slightly higher porosity degree of 0.16 % [114]. A higher substrate temperature during HVOF processing could also contribute to particle oxidation. Nevertheless, it is important to mention that the oxide layers in HVOF coating were thinner and more uniformly distributed between the splats than coatings processed by ASP, not compromising the coating adhesion to the substrate, as shown in Fig. 5c.

In work carried out by Silveira et al. [107], comparing the microstructure of coating processed by HVAF and HVOF, particle temperature of FeMnCrSi feedstock processed by HVAF was found to range between

1440 and 1480 °C, whereas that of the same feedstock processed by HVOF was found to range between 2048 and 2115 °C. With a lower heat input to particles, coatings that HVAF processed developed a reduced oxide content than those processed by HVOF using gas fuel and same chemical composition feedstock. Furthermore, this study found that porosity values in HVAF coatings were very low (0.09–0.14 %), with no systematic variations versus the HVOF ones.

4.2. Factors affecting the coatings hardness and adherence

A summary of the Vickers hardness values recorded for FeMnCrSi coatings (with Ni and B additions) processed by different spraying techniques is shown in Fig. 6.

In studies carried out using HVOF-kerosene fuel and CGS, the hardness increased with the degree of compressive stresses in the coatings. Fig. 6 shows that, for these two processes, the peening effect improved the hardness of the coatings, probably by the increasing cohesion between the splats, and the working hardening effect, as discussed previously. Results also show that for FeMnCrSiNi coatings, processing by CGS tends to produce harder coatings than those processed by ASP or HVOF using gas fuel. Harder coatings can be associated with a higher degree of densification of these coatings, in combination with some degree of working hardening induced during deposition. The addition of Boron in FeMnCrSi coatings deposited by HVOF usually produces harder coatings than PTA. This occurs because PTA coatings consist of coarser recrystallized grains.

In coatings processed by PTA, B addition promotes a significant microstructure change, resulting in a finer inter-dendritic eutectic structure, as seen in Fig. 7. Similar dendritic structures are also present in atomized powders containing B, as seen in the SEM image of a FeMnCrSiB feedstock particle shown in Fig. 8.

The maximum hardness of FeMnCrSi + Ni and FeMnCrSi + B coatings was achieved by HVAF processing. Besides the high level of densification and the presence of oxides, another hypothesis for such high hardness values could be a possible nitrating of the coating induced by processing in N-rich atmosphere. CGS sprayed FeMnCrSi coatings showed hardness above 460 $HV_{0.3}$ and porosity below 0.2 % [50]. This results from a severe cold working by plastic deformation of the particles below their recrystallization temperature [115,116]. This hardness value is close to the measured HVOF-kerosene fuel FeMnCrSi coating, 455 $HV_{0.3}$ [108]. On the downside, coatings processed by CGS showed a much lower adhesion strength to mild steel substrate than coatings processed by ASP and HVOF, as shown in Fig. 5. It indicates that the heating from the above-mentioned thermal spray processes significantly contributes to a superior interfacial bonding, potentially associated with an enhanced inter-diffusion activity between the coating and the substrate.

In FeMnCrSi coatings processed by HVOF using gas fuel, the main factor affecting hardness is the degree of densification, Fig. 9a. In contrast, in FeMnCrSi coatings with B additions processed by PTA, the boron content is the main factor, as illustrated in Fig. 9b.

Many studies indicate HVOF as a suitable method to obtain cavitation-resistant coatings. Its good performance has been attributed to the high kinetic energy of HVOF-sprayed particles, which provides higher adhesion and cohesion between the splats [25,31,117,118]. This was supported by Vaz et al. [87], who compared similar FeMnCrSi alloys feedstock deposited by ASP and HVOF processes, the latter resulting in denser coatings, with the FeMnCrSi0.5B alloy producing a coating with a porosity level below 0.5 %, and well-adhered to the substrate, with an adhesion strength of 48.2 ± 3.0 MPa. This adhesion for thermally sprayed coatings is dependent on the spraying process and parameters; the low-temperature process, in special CGS, uses the high deformation of cold particles and substrate surface during the impact, which promotes an atomic interaction between the materials, called Adiabatic Shear Instability (ASI) [119,120]. However, for higher temperature particles, HVOF, ASP, and Flame Spray, among others, the adherence or bonding to the substrate occurs by mechanical interlocking, atomic interaction, and diffusion of elements, besides micro welding [121,122]. These bonding mechanisms become less effective by increasing the coating thickness, as tensile residual stresses may evolve in the coating. The evolution of residual stresses depends on the process, process parameters and materials, and are determined as results of particle quenching effects, coefficient of thermal expansion mismatch, and peening effect [123,124]. The evolution of tensile residual stresses may limit the thickness of coatings processed by thermal spraying, as it occurs for other techniques such as Physical Vapor Deposition (PVD) [125, 126] and laser cladding [127], among others.

5. Cavitation and wear performance of FeMnCrSi alloys

This section explains the influence of the chemical composition and microstructure on the cavitation resistance of FeMnCrSi coatings. Erosion mechanism and susceptibility to martensitic transformations are also discussed.

The main parameters used to assess the cavitation resistance are the incubation time and maximum erosion rate, which are interpreted from the cumulative mass loss curve of the coatings [128]. The accelerated vibratory cavitation test method ASTM G32-10 [128], and the cavitation liquid jets test method, ASTM G134-95 [129] are the most frequently used cavitation tests to assess the cavitation resistance of different

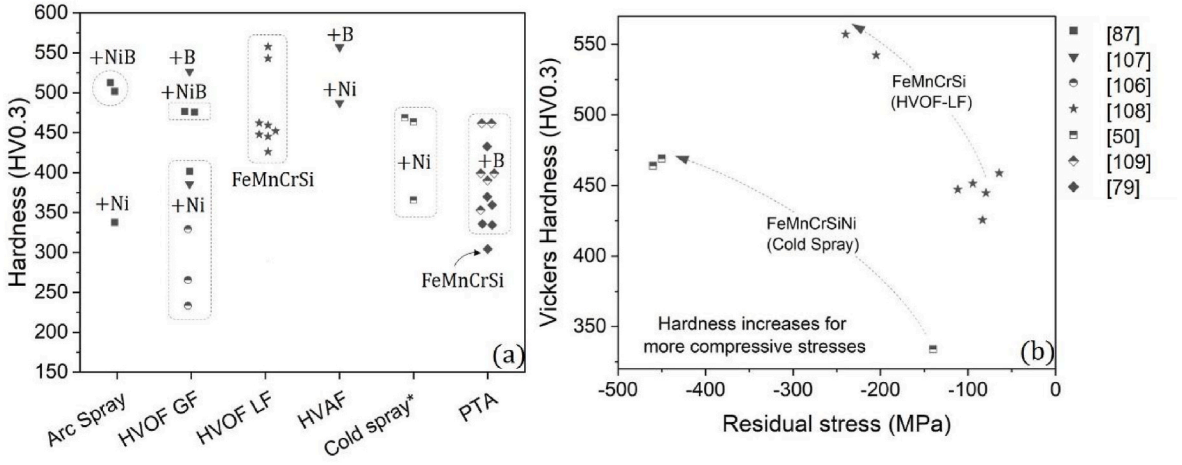

Fig. 6. Hardness of FeMnCrSi coatings, with additions of nickel (+Ni), boron (+B), or Ni and B (+NiB), processed by different spray processes. *Hardness measurements in CGS coatings were carried out with a load of 200 gf (HV0.2).

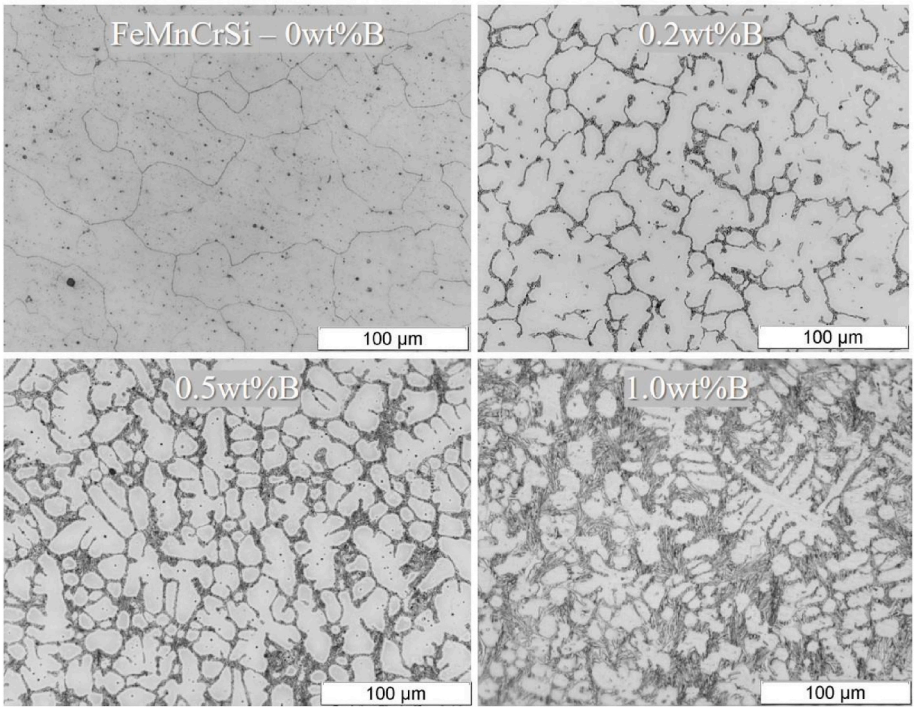

Fig. 7. Microstructure refinement effect of progressive boron additions in FeMnCrSi(B) coatings processed by PTA.

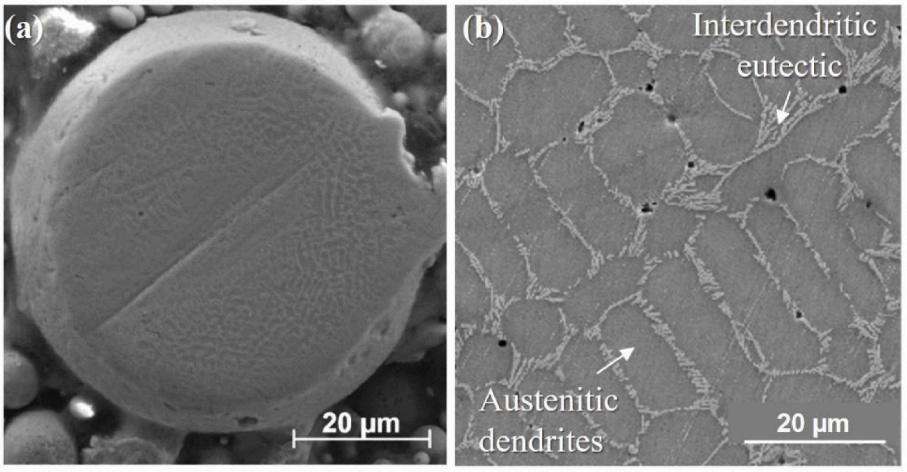

Fig. 8. SEM microstructure images of the FeMnCrSiB alloy containing 0.5 wt% B (a) as-atomized feedstock condition and (b) after PTA processing, showing the presence of significantly finer dendritic structure in the feedstock in comparison to the PTA coating microstructure [107].

materials. The first one is more commonly used because of its simplicity and repeatability of results.

The cavitation media solution is known to influence the specimen cavitation resistance. When using salt water instead of distilled water, the cavitation mass loss tends to be accelerated by a synergy of cavitation and corrosion mechanisms [53,130] To simulate the performance of a coating at a real application more accurately, understanding the environmental conditions may help design non-standardized experiments of greater relevance. An example is presented by Luiz et al. [131] on the corrosion behavior analysis of thermally sprayed coatings used in the Santo Antonio hydropower plant, in which the water collected in the Madera river was used as an electrolyte solution to account for its specificities. In the present work, however, care was taken to include only cavitation results that were carried out in distilled water (to allow for direct comparison in between the results) and that were recorded in accordance with procedures reported in the ASTM G32-10 standard test method [128].

Fig. 10 shows a compilation of cavitation resistance data obtained for FeMnCrSi coatings processed by different spraying techniques. These coatings are compared with other cavitation-resistant commercial coatings (Cavitec, Stellite 6) and bulk materials often used to manufacture runners and other hydraulic machinery.

Results show that the selected spraying processes influenced the cavitation resistance of the FeMnCrSi coatings. It is crucial to observe the erosion mechanism, martensitic transformation susceptibility, and residual stress formation on coatings to understand the cavitation resistance of thermally sprayed coatings. No significant amount of cavitation-induced martensitic transformation was observed in FeMnCrSi coatings processed by HVOF [87,107] or CGS [50], despite their low SFE. The microstructure refinement avoids the strain-induced martensite transformation on cavitated zones [87]. Also, the continuous detachment of splats where ε-martensite may have been formed [107]

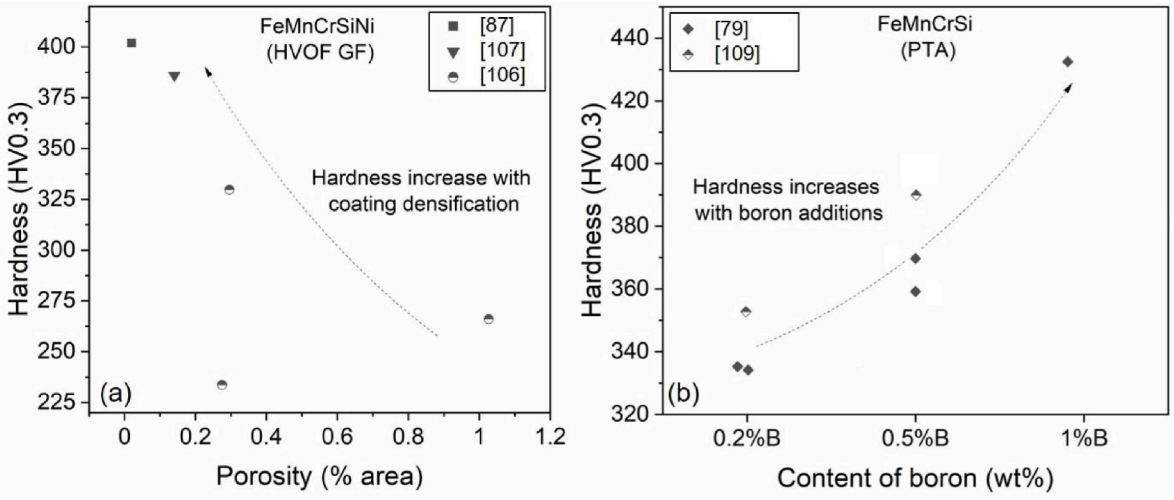

Fig. 9. Increase in hardness with (a) degree of densification in FeMnCrSiNi coatings processed by HVOF gas fuel and (b) the content of B in FeMnCrSi coatings processed by PTA.

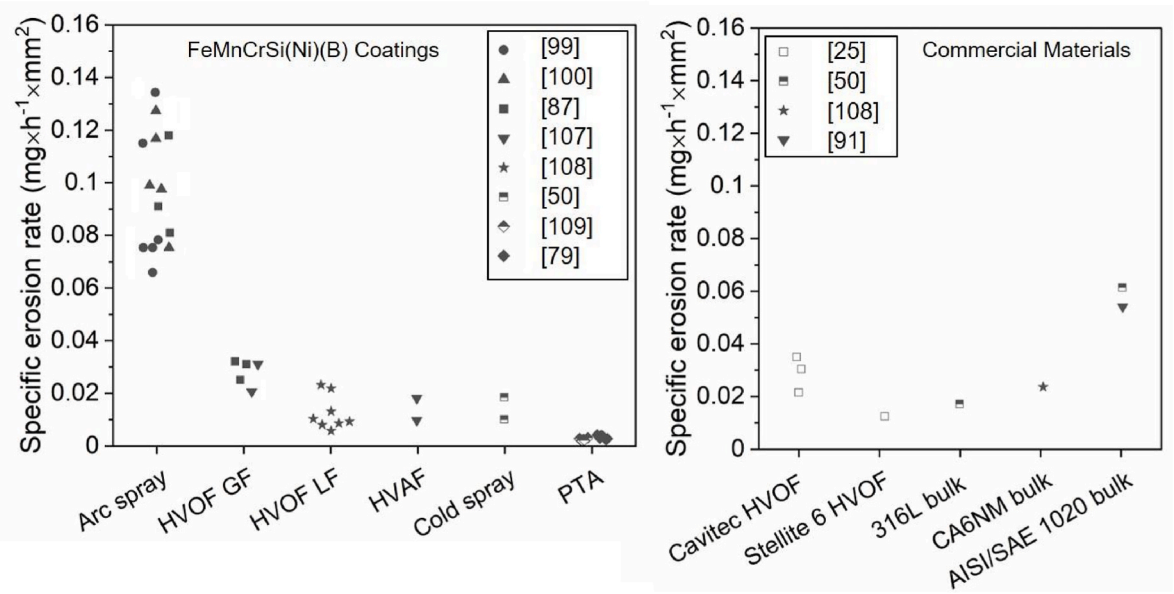

Fig. 10. Specific erosion rate of FeMnCrSi(Ni)(B) coatings processed by different techniques showing competitive performance of coatings processed by high-velocity process (HVOF, HVAF, and CGS) and PTA in comparison to other commercial materials.

can likely reduce the chances of identification of the martensite transformation during the cavitation phenomena. Similarly, no significant cavitation-induced martensitic transformation was observed for FeMnCrSi coating with Ni additions, as illustrated by the XRD diffractograms show in Fig. 11, before and after cavitation. On the other hand, significant fractions of cavitation-induced martensitic transformation were seen in coatings processed by arc spray (TWEA), likely related to its coarser microstructure. However, with the higher content of inter-splat oxide, these coatings showed the highest erosion rate values.

The compressive residual stress collaborates for high-velocity spraying processes to suppress the martensitic transformation. It was reported that austenite transformation to ε-martensite is followed by volume expansion [33]. It relies on a specific lattice ratio, with non-ideal conditions leading to different deformation modes [132]. This way, lattice distortions induced by compressive residual stress could also restrain martensitic transformation and/or other necessary volume changes. Nevertheless, in FeMnCrSi coatings processed by HVOF-kerosene fuel and CGS, compressive residual stresses are beneficial for cavitation resistance, which seems to be associated with improved intersplat cohesion [108].

Significant fractions of cavitation-induced martensitic transformation were observed, however, in FeMnCrSiB coatings processed by HVAF, HVOF and PTA, as seen in Fig. 12. The higher susceptibility of this chemical composition to martensitic transformation can be associated with the lowering of SFE by removal of Cr from solid solution due to the formation of Cr-rich borides [79]. In HVAF coatings, the higher nitrogen concentration can also help reduce the SFE [109]. Because of the inter-splat metallurgical bonding, the FeMnCrSi coatings processed by PTA showed an outstanding cavitation performance, developing the lowest maximum erosion rates and long periods of incubation time, especially the coatings processed with atomized powders. It is worth to mention that, besides having a high cavitation resistance, coatings processed by PTA are usually thicker, which can further increase the lifetime of the thermally sprayed coating. Nevertheless, as mentioned earlier, the total thickness may be limited by the evolution of tensile

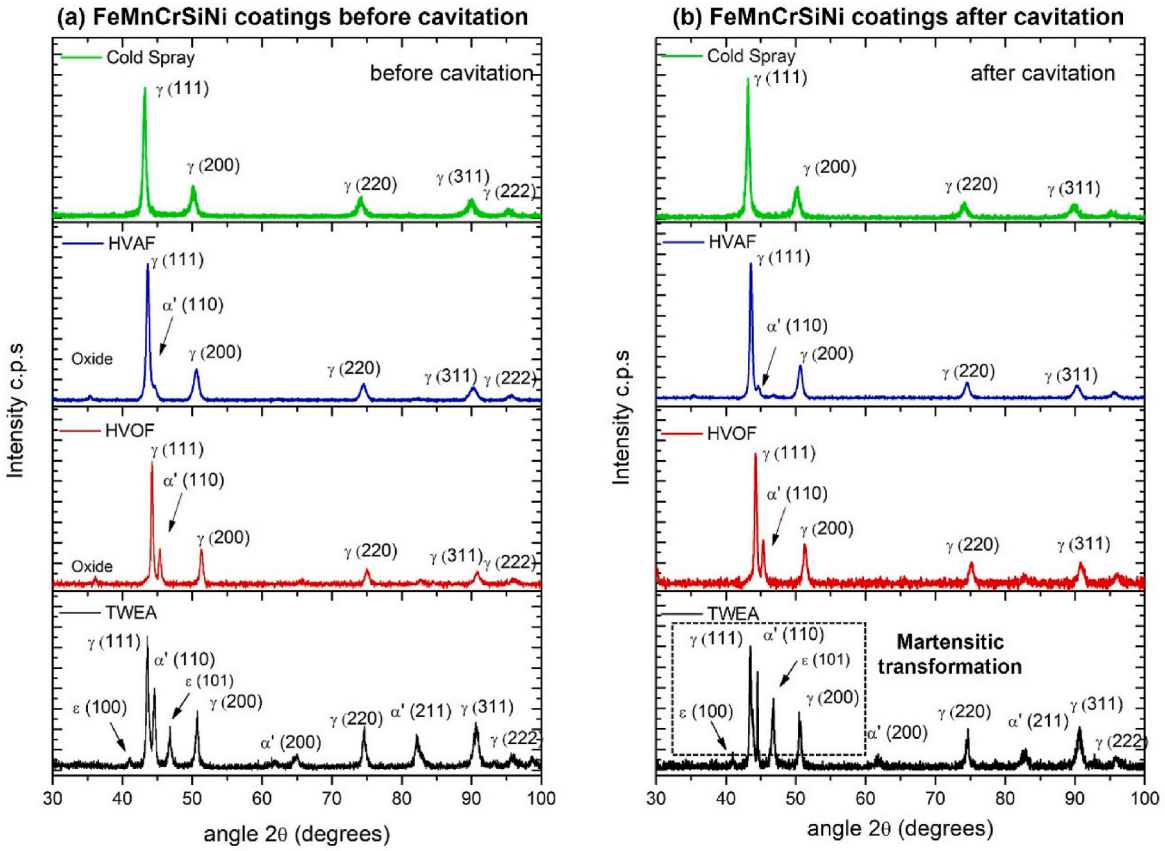

Fig. 11. XRD analysis of FeMnCrSiNi coatings processed by (top) cold spray, HVAF, HVOF and (bottom) TWEA arc spray showing no significant cavitation-induced martensitic transformation in coatings processed by high-velocities thermal spray techniques, in contrast with significant strain-induced martensitic transformation in coatings processed by TWEA after cavitation.

residual stresses on the surface.

Fig. 13a,d shows that coatings processed by ASP and CGS fail predominantly by splat detachment. For the first one, the cohesion was compromised by the presence of inter-splat oxides. Despite having the same predominant erosion mechanism, sufficient cohesion could be achieved in CGS coatings to achieve competitive performance. Fig. 13b and c shows that coatings processed by HVOF and HVAF fail as a combination of splat fracture and splat detachment mechanisms. In coatings processed PTA, the complete melting of the particles promotes the formation of a metallurgical bonding, significantly reducing the erosion rate, Fig. 13e and f. As seen in Fig. 13e, in PTA coatings containing boron the erosion starts predominantly at the eutectic region. The use of atomized powders increases the formation of slip lines as a result of the cavitation induced martensitic transformation, as shown in Fig. 13f.

Coatings processed by ASP, HVOF, HVAF, and CGS did not show an incubation period. This is associated with the typical inter-splat mechanical bonding that causes splat to detach before plastic deformation mechanisms reach their total capacity. This effect is illustrated in Fig. 14. Silveira et al. [107] showed that FeMnCrSi coatings processed by HVOF and HVAF have a higher erosion rate during the initial minutes cavitation, indicating a higher susceptibility of the outermost layers to fracture or detachment. In coatings processed by PTA; however, in which the bonding is metallurgical, plastic mechanisms are more fully exploited. In coatings processed with mechanical mixtures of elemental powders, the average incubation period was about 8–9 h. In coatings processed with atomized powders, the martensitic transformation mechanism contributed towards the obtention of average incubation periods higher than 23 h [79].

The evaluation of the FeMnCrSiB feedstock powder preparation process on the coating properties was studied, by depositing FeMnCrSiB coatings with similar chemical composition but obtained by gas atomization or milling of pre-alloyed powders (Fe, Fe–Mn, Cr, FeCrN, Mn, Si, and Fe–B), with a particle size distribution smaller than 180 μm. For milling, FeMnCrSi alloys with four nominal boron contents, 0, 0.2, 0.5, and 1.0 wt%B (Fig. 5) were prepared, while for gas atomizing, two nominal B contents, 0.2 and 0.5 wt%B were investigated [79]. The B addition increases the hardness of the FeMnCrSi PTA coatings from 300 to 420 HV contributing to a systematic reduction in the maximum erosion rate. The addition of B in Fe-based alloy was also shown to improve the abrasion wear performance, as reported by Kim et al. [133]. The total mass loss in the rubber wheel testing, ASTM G65-00 [134], decreased dramatically with boron concentration up to 0.6 wt%B, associated with microstructure refinement, precipitation of primary borides, strengthening of the γ-austenite matrix, and a hardness increase from about 400 up to 950 HV, for 2.0 wt%B additions.

It was also shown that processing of FeMnCrSiB coatings using gas atomized feedstock instead of milled powders further refine the coating microstructure, impacting beneficially on the cavitation resistance and performance. Similarly, in Fe-based alloys, an improvement in the cavitation resistance with B and Mn additions was also reported by Kim et al. [66], attributing this resistance improvement to γ→ε, which is a more straightforward mechanism than γ→α', and promotes the cavitation resistance by the energy absorption rather than dislocation motion. Using a mixture of elemental powders as raw material but without B addition, Ribeiro et al. [28] presented FeMnCrSi alloys with higher cavitation resistance than other alloys usually deposited by the welding on hydraulic runners.

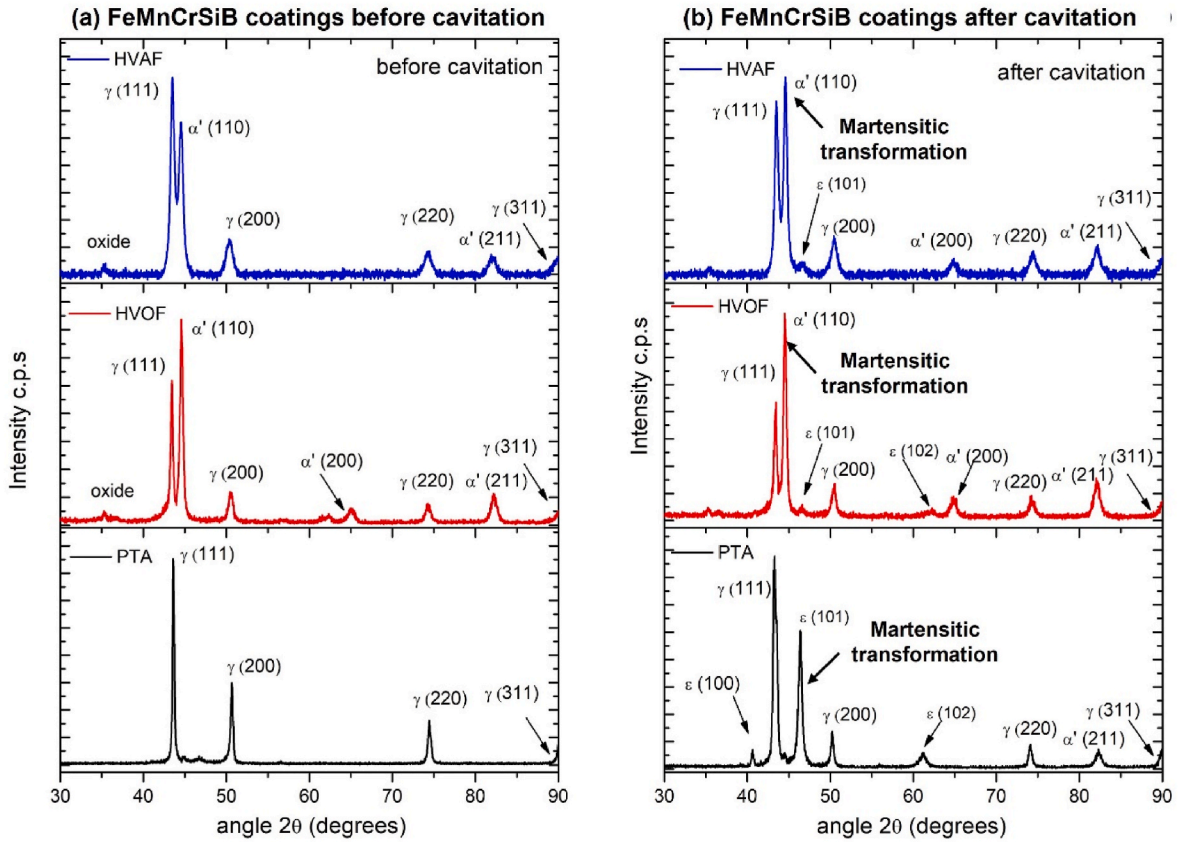

Fig. 12. XRD analysis of FeMnCrSiB coatings processed by (top) HVAF, HVOF and (bottom) PTA showing the higher susceptibility of this chemical composition to undergo strain-induced martensitic transformation during cavitation as an energy absorption mechanism before fracture.

6. Summary and outlook

A bibliometric study is a valuable tool for conducting a systematic literature review and observing the results presented by many authors [135,136]. This may provide a direction for future research based on the literature published in the high-performance materials field to keep pushing the frontier of knowledge in the research of Co-free FeMn stainless steel coatings, such as FeMnCrSi.

Using the Scopus database limited to the years between 2000 and 2022, the search was restricted to articles, conference papers, and book chapters, only covering their title, abstract, or keywords fields. The searching terms were (cavitation AND resistant AND coating*) OR (cavitation AND resistant AND thermal AND spray*) OR (cavitation AND resistant AND cladding*) OR (femncrsi) OR (femn AND coating*) OR (cavitation AND hvof) OR (erosion AND thermal AND spray*) OR (corrosion AND thermal AND spray*). A filter regarding the subject areas was applied, considering publications only in "materials science" OR "chemistry" OR "engineering" OR “chemical engineering” OR “environmental science”. The search query found a total of 4901 documents. Fig. 15 presents the number of works published annually since 2000, indicating an increasing trend, reaching a maximum of 406 works in 2022. The FeMnCrSi cavitation resistant coatings have grown its participation in this number of publications per year, reaching 15 works in 2019, which suggests an increase in the scientific community’s interest in this theme.

Even though there are many published works associated with this work, in no way does it exhaust the vast literature dedicated to the study of improving the material resistance against wear and cavitation erosion, especially for FeMnCrSi coating. The most recent publications indicate many possibilities for the deposition of FeMnCrSi coatings, using different processes or the promising use of post-treatment. Using low-oxidation and high-velocity processes improves the wear resistance of the coatings. Compared to ASP process, lower chemical decomposition and higher hardness of these coatings.

The feasibility of depositing FeMnCrSi coatings by various techniques has been demonstrated, with each process having its particular advantages. The ASP is portable and suitable equipment to deposit thermally sprayed coating in hydropower plants and large equipment, especially considering its high deposition rate. However, the HVOF process has important microstructural advantages, such as higher density, hardness, and splats cohesion. Similarly, coatings processed by the CGS technique present high density and almost no oxidation. Coatings processed by PTA achieve high cavitation resistance and long incubation time. However, dilution with the base metal must be controlled using tuning PTA parameters to maintain suitable chemical composition.

In summary, each process has its pros and cons, but this review evidences the viability of each one of them. Even the coatings processed by ASP, which showed relatively lower cavitation resistance, have cavitation resistance similar to that of low-carbon steel, Fig. 10, a substrate material for many runners. However, when the CA6NM stainless steel is used as a reference, the HVOF or CGS sprayed coatings are the most indicated to repair or improve the component cavitation resistance, alongside with FeMnCrSi coatings processed by PTA.

7. Further developments

Further developments in the topic of FeMnCrSi wear and cavitation resistant coatings include the use different processing techniques as well as the use of post-processing techniques.

Although the use of small PTA torches to repair worn areas of large hydraulic runners has been validated at laboratory level as an alternative to the extensively used arc-welding process, whose high heat inputs

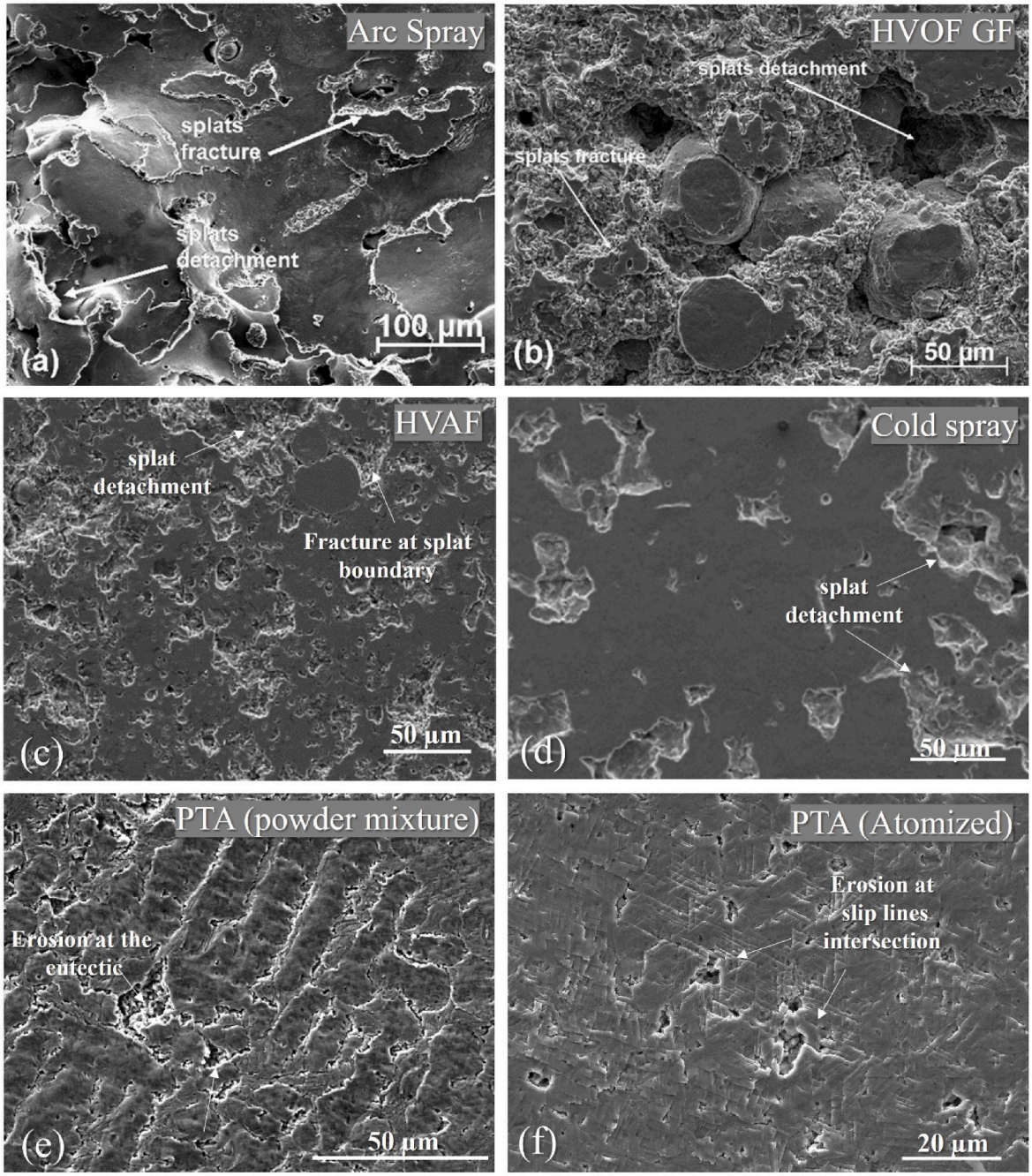

Fig. 13. Erosion mechanism of (a) FeMnCrSi coatings processed by arc spray and (b) HVOF gas fuel, after 1 h of cavitation; (c) FeMnCrSiNi coating processed by HVAF after 1 h of cavitation; (d) FeMnCrSi coating processed by CGS after 1 h of cavitation; (e) FeMnCrSi0.5B coating processed by PTA with mechanical mixtures of elemental powers after over 12 h of cavitation; (f) FeMnCrSi0.5B coating processed PTA using atomized powders after 11 h of cavitation. In (a) and (d), coating processed by ASP and CGS fails predominantly by splat detachment. Coatings processed by HVOF and HVAF fail as a combination of splat fracture and splats detachment mechanisms, (b) and (c). Coatings processed by PTA using mechanical mixtures of elemental powders containing boron, like (e), erosion starts predominantly at the eutectic region. In coatings processed by PTA using atomized powders like (f), abundant slip line formation is seen as a result of martensitic transformation, with erosion occurring predominantly at their intersections [29,50,79,87].

can be deleterious for the mechanical properties and toughness of the runners, martensitic stainless steels in particular [11,16], the use of arc welding has a considerable advantage of high production and reduced repair time of runners. Furthermore, with the development of new arc-welding parameters control systems, such as the Cold Metal Transfer (CMT), low levels of dilution and tensile residual stress can be achieved [137–141]. Although promissing, studies on processing of FeMn or FeCr alloys using this technique are still scarce.

The laser process is another technique to be explored regarding the wear and cavitation performance of FeMnCrSi coatings. Different FeMn and FeCr alloys deposited by different laser deposition techniques were studied [142,143]. Microstructure, residual stress formation [144,145], or heat treatment influence of as-weld material or friction wear resistance of FeMnCrSi were studied [146–148]. However, there is a lack in the literature regarding the cavitation and erosion performance of FeMnCrSi coatings produced by laser cladding, which is a very promisor process, mainly because of the low oxidation in comparison to PTA or other welding processes. As PTA, laser cladding has metallurgic bonding

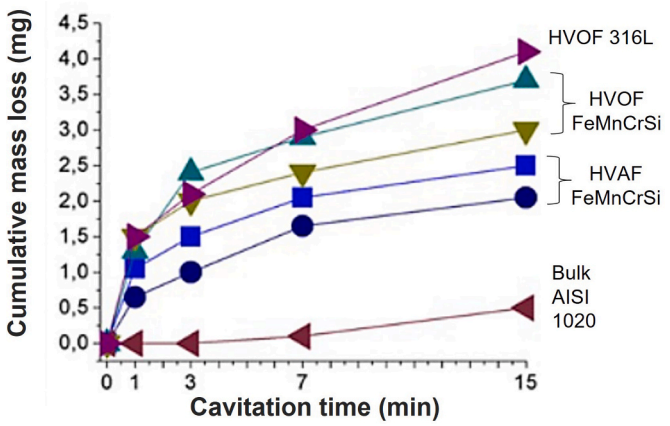

Fig. 14. Cumulative mass loss of FeMnCrSi coatings processed by HVOF and HVAF illustrating the higher erosion rate in the initial minutes of the cavitation test associated with weaker inter-splat bonding of the outermost layers to due the absence of compaction by successive layers [107].

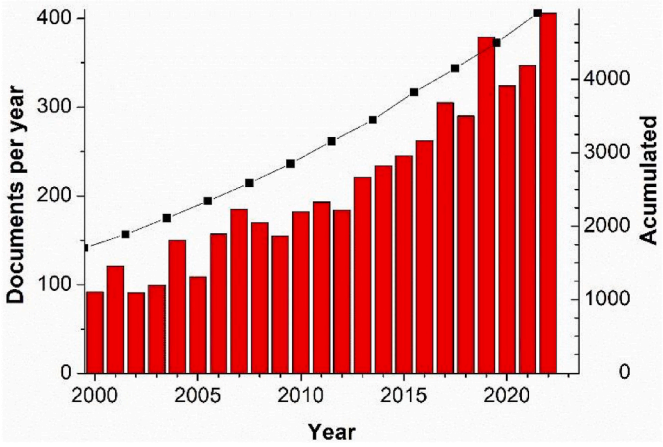

Fig. 15. Number of documents annually published in the cavitation and wear-resistant coatings subject.

with the substrate, a lower substrate dilution, and a smaller heat-affected zone [149]. The development of high-speed laser cladding technology increased the industrial application field of this technology, which can be used to deposit FeMnCrSi alloys. Liu et al. [143] observed the formation of the ε-martensite phase due to the stress self-accommodation effect. This effect occurs due to the residual stress generated by the laser cladding process, inducing a unit cell deformation to reduce residual stress, which may improve the cavitation resistance of FeMnCrSi coatings because the mass loss by cavitation is related to the material's fatigue performance. Lower tensile residual stress improves the material's fatigue life [48,51,78,149].

Alternatively to laser processing, PTA remelting post-treatment of the FeMnCrSi alloys coatings promoted extreme changes in the material. The porosity decreased from 1.1 % to zero, and the oxide content decreased from 18.2 % to less than 0.5 %. This occurred due to the densification of the coating and elimination of the oxides by vaporization and slag flotation. Microstructural changes impact the hardness of the coating, rising from 264 to 320 HV, affecting the coating performance [150]. Another aspect that can improve the wear resistance of FeMnCrSi is the precipitation of second-phase particles that can be dispersed in the austenite matrix. In work by Bu et al. [146], wear resistance was enhanced due to the strengthening of second-phase particles, with prior deformation, especially under heavy load conditions. It stimulates the studies of new post-processing treatments. Laser remelting of thermally sprayed coatings is a novelty to be explored due to its low and controlled dilution, saving the heat-sensitive runners' martensitic stainless steel.

The effect of work-hardening on cavitation resistance of FeMnCrSi coatings processed by PTA was assessed by Cruz et al. [109]. Testing of samples with and without cold work deformation induced by machining operations demonstrated the effectiveness of plastic deformation or cold working on improving the cavitation resistance of FeMnCrSi PTA coatings, as seen in Fig. 16. Cold work was found to generate abundant slip lines as result of stain induced phase transformation, contributing to increase the coating hardness from 353 to 462 HV, and to reduce the maximum erosion rate.

Usually, high kinetic energy thermal spraying techniques can cause compressive stresses at the surface, increasing the density and hardness of these coatings. However, the sprayed surface inevitably has many crystalline defects due to the particles' impact during deposition. Plasma nitriding Glow Discharge (GD) can modify the microstructure and improve the surface properties, extracting the maximum potential of the alloy for a given application. It is well known that Ni-based alloys can be nitrided successfully, resulting in nitrogen-expanded austenite (γ_N or S-phase). Expanded austenite provides high corrosion, wear resistance, and improves surface mechanical properties [151]. However, the cavitation resistance performance depends on a more profound investigation.

The work conducted by Park et al. [152] showed that the 316 stainless steel HVOF coating (FCC) had the thinnest nitride layer. Meanwhile, the 410 stainless steel coating (BCC) had the thickest nitride layer. Plasma-nitrocarburized coating samples had a thicker nitrided layer than the plasma-nitrided coating samples. The nitriding and nitrocarburizing surfaces showed microhardness above 1300 HV, three times greater than as-sprayed coatings. The authors indicated that the precipitation of CrN with Fe_3N and Fe_4N improved the surface hardness of the coatings. Therefore, a significant potential increase in FeMnCrSi alloys applications can be made by introducing laser deposition, heat treatment, and nitriding thermochemical treatment to guarantee properties that industrial users practice.

In summary, post-treatments of FeMnCrSi coatings can promote a better cavitation wear resistance. The wear mechanisms are strongly influenced by the material surface condition, such as roughness or geometry, and the material properties, such as hardness and fracture toughness. The post-processing treatments presented in the literature were shown to change the FeMnCrSi coatings surface and improve cavitation resistance using severe metallurgical intervention, remelting, or mechanical treatments, such as shot-peening and cold-working. However, thermo-chemical post-treatments were still not evaluated, and promising developments could be expected with boriding or nitriding to innovate in the study of FeMnCrSi alloys.

Although initially developed as cavitation resistant coatings, the FeMnCrSi alloys addressed in this study have a high potential to withstand other types of wear, such as solid particle erosion, sliding, or friction, for example, due to their hardness and metallurgical characteristics of low SFE, TRIP, and TWIP mechanisms. In this way, the development of studies aiming at other wear testing and application is foreseen.

Data availability

Data will be made available on request.

CRediT authorship contribution statement

Rodolpho F. Vaz: Conceptualization, Data curation, Investigation, Methodology, Supervision, Writing – original draft, Writing – review & editing. **Luciana L. Silveira:** Investigation, Methodology, Writing – review & editing. **Juliane R. Cruz:** Data curation, Formal analysis, Investigation, Methodology, Writing – review & editing. **Anderson G.**

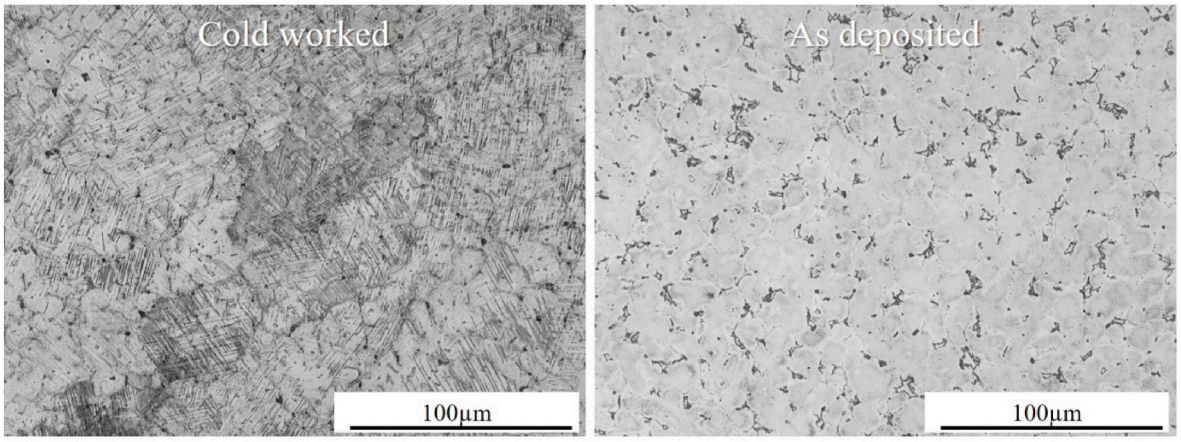

Fig. 16. Optical microscopy microstructure of coatings processed with elemental powders showing B content effect on the growth of secondary dendritic arms and increasing of eutectic amount [79].

M. Pukasiewicz: Conceptualization, Investigation, Methodology, Supervision, Writing – review & editing.

Declaration of competing interest

The authors declare the following financial interests/personal relationships which may be considered as potential competing interests:

The Co-author Juliane Ribeiro da Cruz is a member of the Early Career Advisory Board of the Journal Surface and Coatings Technology.

Acknowledgements

Authors gratefully acknowledge Copel Energia and the Agência Nacional de Energia Elétrica (ANEEL) for R&D funding. Authors would like to thank LACTEC, the Federal University of Parana (UFPR), the Federal University of Technology – Parana (UTFPR) and the University of Barcelona for institutional support. Authors are grateful to Professor Sanjay Sampath from the Center for Thermal Spray Research (CTSR) of the State University of New York and to Stefan Björklund from the University West for their collaborations. Support from the C^2MMa laboratory from the Federal University of Technology - Parana is greatfully acknowledged.

References

[1] R. Ehrlich, H.A. Geller, Hydropower, in: Renewable Energy, CRC Press, Boca Raton, FL, USA, 2018, pp. 221–248.
[2] C.S. Kaunda, C.Z. Kimambo, T.K. Nielsen, Hydropower in the context of sustainable energy supply: a review of technologies and challenges, ISRN Renew. Energy 2012 (2012) 1–15, https://doi.org/10.5402/2012/730631.
[3] A.S. Azad, S.A. Rahaman, J. Watada, P. Vasant, J.A.G. Vintaned, Optimization of the hydropower energy generation using meta-heuristic approaches: a review, Energy Rep. 6 (2020) 2230–2248, https://doi.org/10.1016/j.egyr.2020.08.009.
[4] E. Sperling, Von hydropower in Brazil: overview of positive and negative environmental aspects, Energy Proc. 18 (2012) 110–118, https://doi.org/10.1016/j.egypro.2012.05.023.
[5] E.J. Arbuckle, M. Binsted, E.G.R. Davies, D.V. Chiappori, C. Bergero, M. Siddiqui, C. Roney, H.C. Mcjeon, Y. Zhou, N. Macaluso, Insights for Canadian electricity generation planning from an integrated assessment model: should we Be more cautious about hydropower cost overruns? Energy Pol. 150 (2021) 1–13, https://doi.org/10.1016/j.enpol.2021.112138.
[6] X. Li, Z. Chen, X. Fan, Z. Cheng, Hydropower development situation and prospects in China, Renew. Sustain. Energy Rev. 82 (2018) 232–239, https://doi.org/10.1016/j.rser.2017.08.090.
[7] T. Sakabe, T. Murakawa, K. Nishida, J. Ide, T. Sato, Trend analyses of the small and medium hydro power development after the FIT scheme introduced in Japan, Energy Rep. 6 (2020) 358–363, https://doi.org/10.1016/j.egyr.2020.11.230.
[8] I.A. Adejumobi, D.I. Shobayo, Optimal selection of hydraulic turbines for small hydro electric power generation – a case study of opeki river, south western Nigeria, Niger. J. Technol. 34 (2015) 530–537, https://doi.org/10.4314/njt.v34i3.15.
[9] K. Sakulphan, E.L.J. Bohez, A new optimal selection method with seasonal flow and irrigation variability for hydro turbine type and size, Energies 11 (2018) 1–16, https://doi.org/10.3390/en11113212.
[10] P. Breeze, Hydropower, in: P. Breeze (Ed.), Power Generation Technologies, Newnes, Oxford, 2019, pp. 173–201.
[11] S.S.M. Tavares, C.R. Rodrigues, J.M. Pardal, E. da S. Barbosa, H.F.G. de Abreu, H. F.G. de Abreu, Effects of post weld heat treatments on the microstructure and mechanical properties of dissimilar weld of supermartensític stainless steel, Mater. Res. 17 (2014) 1336–1343, https://doi.org/10.1590/1516-1439.299314.
[12] D. Carrouge, H.K.D.H. Bhadeshia, P. Woollin, Effect of δ -ferrite on impact properties of supermartensitic stainless steel heat affected zones, Sci. Technol. Weld. Join. 9 (2004) 377–389, https://doi.org/10.1179/136217104225021823.
[13] J.F. Santa, J.A. Blanco, J.E. Giraldo, A. Toro, Cavitation erosion of martensitic and austenitic stainless steel welded coatings, Wear 271 (2011) 1445–1453, https://doi.org/10.1016/j.wear.2010.12.081.
[14] D. Thibault, P. Bocher, M. Thomas, J. Lanteigne, P. Hovington, P. Robichaud, Reformed austenite transformation during fatigue crack propagation of 13% Cr–4%Ni stainless steel, Mater. Sci. Eng. A 528 (2011) 6519–6526, https://doi.org/10.1016/j.msea.2011.04.089.
[15] R. de Paula Silva, M.I.S.T. Faria, L.F.C.B. de Almeida, C.A. Nunes, D. Vieira, W. Borges, Microstructure and mechanical properties of ASTM A743 CA6NM steel welded by FCAW process, Mater. Res. 20 (2017) 1622–1629, https://doi.org/10.1590/1980-5373-MR-2017-0468.
[16] R.F. Váz, R. Tristante, A.G.M. Pukasiewicz, A.R. Capra, A. Chicoski, C.G. Filippin, R.S.C. Paredes, S.L. Henke, Welding and thermal spray processes for maintenance of hydraulic turbine runners: case studies, Soldag. Inspeção 26 (2021) 1–13, https://doi.org/10.1590/0104-9224/si25.40.
[17] M.K. Padhy, R.P. Saini, A review on silt erosion in hydro turbines, Renew. Sustain. Energy Rev. 12 (2008) 1974–1987, https://doi.org/10.1016/j.rser.2007.01.025.
[18] H. Kumar, C. Chittosiya, V.N. Shukla, HVOF sprayed WC based cermet coating for mitigation of cavitation, erosion & abrasion in hydro turbine blade, Mater. Today Proc. 5 (2018) 6413–6420, https://doi.org/10.1016/j.matpr.2017.12.253.
[19] H. Zhang, Y. Gong, X. Chen, A. McDonald, H. Li, A comparative study of cavitation erosion resistance of several HVOF-sprayed coatings in deionized water and artificial seawater, J. Therm. Spray Technol. 28 (2019) 1060–1071, https://doi.org/10.1007/s11666-019-00869-x.
[20] L.A. Espitia, A. Toro, Cavitation resistance, microstructure and surface topography of materials used for hydraulic components, Tribol. Int. 43 (2010) 2037–2045, https://doi.org/10.1016/j.triboint.2010.05.009.
[21] C.E. Brennen, Cavitation and Bubble Dynamics, Cambridge University Press, New York, NY, USA, 2013.
[22] J.-P. Franc, J.-M. Michel, *Fundamentals of Cavitation*; Fluid Mechanics and its Applications, vol. 76, Kluwer Academic Publishers, Dordrecht, 2005.
[23] L. Bai, J. Yan, Z. Zeng, Y. Ma, Cavitation in thin liquid layer: a review, Ultrason. Sonochem. 66 (2020) 1–9, https://doi.org/10.1016/j.ultsonch.2020.105092.
[24] U. Dorji, R. Ghomashchi, Hydro turbine failure mechanisms: an overview, Eng. Fail. Anal. 44 (2014) 136–147, https://doi.org/10.1016/j.engfailanal.2014.04.013.
[25] S. Lavigne, F. Pougoum, S. Savoie, L. Martinu, J.E. Klemberg-Sapieha, R. Schulz, Cavitation erosion behavior of HVOF CaviTec coatings, Wear 386–387 (2017) 90–98, https://doi.org/10.1016/j.wear.2017.06.003.
[26] R. Singh, S.K. Tiwari, S.K. Mishra, Cavitation erosion in hydraulic turbine components and mitigation by coatings: current status and future needs, J. Mater. Eng. Perform. 21 (2012) 1539–1551, https://doi.org/10.1007/s11665-011-0051-9.
[27] Z. Xiaojun, L.A.J. Procopiak, N.C. Souza, A.S.C.M. D'Oliveira, Phase transformation during cavitation erosion of a Co stainless steel, Mater. Sci. Eng. A 358 (2003) 199–204, https://doi.org/10.1016/S0921-5093(03)00297-1.

[28] H.O. Ribeiro, A.J. de A. Buschinelli, J.C. Dutra, A.S.C.M. D'Oliveira, Resistência à Erosão Por Cavitação de Aços Inoxidáveis Austeníticos CrMnSiN Depositados Por PTA, Soldag. Inspeção 15 (2010) 121–129, https://doi.org/10.1590/S0104-92242010000200006.

[29] Z. Wang, J. Zhu, Effect of phase transformation on cavitation erosion resistance of some ferrous alloys, Mater. Sci. Eng. A 358 (2003) 273–278, https://doi.org/10.1016/S0921-5093(03)00306-X.

[30] F. Wantang, Z. Yangzeng, J. Tianfu, Y. Mei, Structural changes after cavitation erosion for a Cr-Mn-N stainless steel, Wear 205 (1997) 28–31, https://doi.org/10.1016/S0043-1648(96)07262-6.

[31] W. Yuping, L. Pinghua, C. Chenglin, W. Zehua, C. Ming, H. Junhua, Cavitation erosion characteristics of a Fe–Cr–Si–B–Mn coating fabricated by high velocity oxy-fuel (HVOF) thermal spray, Mater. Lett. 61 (2007) 1867–1872, https://doi.org/10.1016/j.matlet.2006.07.147.

[32] J.C. Li, M. Zhao, Q. Jiang, Alloy design of FeMnSiCrNi shape-memory alloys related to stacking-fault energy, Metall. Mater. Trans. A 31 (2000) 581–584, https://doi.org/10.1007/s11661-000-0001-x.

[33] Q. Lai, P. Song, H. Zhou, L. Xiao, T. Feng, C. Li, Deformation-induced martensitic transformation and strain hardening in a nanocrystalline FeMn alloy processed by severe austenite pre-deformation, Materialia 13 (2020), 100832, https://doi.org/10.1016/j.mtla.2020.100832.

[34] F. Pöhl, S. Mottyll, R. Skoda, S. Huth, Evaluation of cavitation-induced pressure loads applied to material surfaces by finite-element-assisted pit analysis and numerical investigation of the elasto-plastic deformation of metallic materials, Wear 330–331 (2015) 618–628, https://doi.org/10.1016/j.wear.2014.12.048.

[35] S.C. Roy, J.-P. Franc, C. Pellone, M. Fivel, Determination of cavitation load spectra – Part 1: static finite element approach, Wear 344–345 (2015) 110–119, https://doi.org/10.1016/j.wear.2015.09.006.

[36] L. Ye, X. Zhu, Y. He, X. Wei, Ultrasonic cavitation damage characteristics of materials and a prediction model of cavitation impact load based on size effect, Ultrason. Sonochem. 66 (2020), 105115, https://doi.org/10.1016/j.ultsonch.2020.105115.

[37] N. Suman, S.C. Roy, Cyclic behavior of material after single loading of cavitation peening, Mater. Today Proc. 62 (2022) 7480–7486, https://doi.org/10.1016/j.matpr.2022.03.508.

[38] Y.Z. Li, M. Wang, M.X.I. Huang, Measurement of plastic strain in martensite matrix induced by austenite-to-martensite transformation In-Situ Measurement of Plastic Strain in Martensite Matrix Induced by Austenite-to-Martensite Transformation, Mater. Sci. Eng. A 811 (2021), 141061, https://doi.org/10.1016/j.msea.2021.141061.

[39] I. Janeiro, O. Hubert, J.-H. Schmitt, In-situ strain induced martensitic transformation measurement and consequences for the modeling of medium Mn stainless steels mechanical behavior, Int. J. Plast. 154 (2022), 103248, https://doi.org/10.1016/j.ijplas.2022.103248.

[40] Z. Feng, M. Zecevic, M. Knezevic, Stress-assisted (Γ→α′) and strain-induced (Γ→ε→α′) phase transformation kinetics laws implemented in a crystal plasticity model for predicting strain path sensitive deformation of austenitic steels, Int. J. Plast. 136 (2021), 102807, https://doi.org/10.1016/j.ijplas.2020.102807.

[41] G.B. Olson, M. Cohen, A mechanism for the strain-induced nucleation of martensitic transformations, J. Less Common Met. 28 (1972) 107–118, https://doi.org/10.1016/0022-5088(72)90173-7.

[42] V.M. Schastlivtsev, M.A. Filippov, Role of the Bogachev - Mints concept of metastability of austenite in choosing wear-resistant materials, Met. Sci. Heat Treat. 47 (2005) 3–5, https://doi.org/10.1007/s11041-005-0020-8.

[43] G.Y. Koga, W. Wolf, R. Schulz, S. Savoie, C. Bolfarini, C.S. Kiminami, W.J. Botta, Corrosion and wear properties of FeCrMnCoSi HVOF coatings, Surf. Coatings Technol. 357 (2019) 993–1003, https://doi.org/10.1016/j.surfcoat.2018.10.101.

[44] Z. Wang, J. Zhu, Cavitation erosion of Fe–Mn–Si–Cr shape memory alloys, Wear 256 (2004) 66–72, https://doi.org/10.1016/S0043-1648(03)00393-4.

[45] D. Raabe, B. Sun, A. Kwiatkowski Da Silva, B. Gault, H.W. Yen, K. Sedighiani, P. Thoudden Sukumar, I.R. Souza Filho, S. Katnagallu, E. Jägle, et al., Current challenges and opportunities in microstructure-related properties of advanced high-strength steels, Metall. Mater. Trans. A Phys. Metall. Mater. Sci. 51 (2020) 5517–5586, https://doi.org/10.1007/s11661-020-05947-2.

[46] L. Patnaik, S. Ranjan Maity, S. Kumar, Status of nickel free stainless steel in biomedical field: a review of last 10 Years and what else can Be done, Mater. Today Proc. 26 (2020) 638–643, https://doi.org/10.1016/j.matpr.2019.12.205.

[47] Hong, Z.; Hang, X.; Zai Mei, L.; Qian Yun, L.; Shao Hong, C.; Lei, Z. Study of Migration and Safety Assessment of Manganese (Mn) from Food Contact Stainless-Steel Products in China., doi:10.3967/bes2022.048.

[48] A. Thiruvengadam, S. Waring, Mechanical properties of metals and their cavitation-damage resistance, J. Sh. Res. 10 (1966) 1–9, https://doi.org/10.5957/jsr.1966.10.1.1.

[49] M.I. Pashechko, Wear resistance of eutectic coatings of the Fe–Mn–C–B system alloyed with Si, Ni, and Cr, Mater. Sci. 46 (2011) 695–701, https://doi.org/10.1007/s11003-011-9342-4.

[50] A.G.M. Pukasiewicz, W.R. de Oliveira, R.F. Váz, G.B. de Souza, F.C. Serbena, S. Dosta, I.G. Cano, Influence of the deposition parameters on the tribological behavior of cold gas sprayed FeMnCrSi alloy coatings, Surf. Coatings Technol. 428 (2021), 127888, https://doi.org/10.1016/j.surfcoat.2021.127888.

[51] R.H. Richman, W.P. McNaughton, Correlation of cavitation erosion behavior with mechanical properties of metals, Wear 140 (1990) 63–82, https://doi.org/10.1016/0043-1648(90)90122-Q.

[52] D.E. Zakrzewska, A.K. Krella, Cavitation erosion resistance influence of material properties, Adv. Mater. Sci. 19 (2019) 18–34, https://doi.org/10.2478/adms-2019-0019.

[53] Y. Tian, H. Zhao, R. Yang, X. Liu, X. Chen, J. Qin, A. McDonald, H. Li, In-situ SEM investigation on stress-induced microstructure evolution of austenitic stainless steels subjected to cavitation erosion and cavitation erosion-corrosion, Mater. Des. 213 (2022), 110314, https://doi.org/10.1016/j.matdes.2021.110314.

[54] G. Bregliozzi, A.D.I. Schino, H. Haefke, J.M. Kenny, Cavitation erosion resistance of a high nitrogen austenitic stainless steel as a function of its grain size, J. Mater. Sci. Lett. 22 (2003) 981–983, https://doi.org/10.1023/A:1024673215823.

[55] C.J. Heathcock, B.E. Protheroe, A. Ball, Cavitation erosion of stainless steels, Wear 81 (2006) 311–327, https://doi.org/10.1016/0043-1648(82)90278-2.

[56] J. Stella, E. Schüller, C. Heßing, O.A. Hamed, M. Pohl, D. Stöver, Cavitation erosion of plasma-sprayed NiTi coatings, Wear 260 (2006) 1020–1027, https://doi.org/10.1016/j.wear.2005.06.002.

[57] J.H. Kim, K.S. Na, G.G. Kim, C.S. Yoon, S.J. Kim, Effect of manganese on the cavitation erosion resistance of iron–chromium–carbon–silicon alloys for replacing cobalt-base stellite, J. Nucl. Mater. 352 (2006) 85–89, https://doi.org/10.1016/j.jnucmat.2006.02.072.

[58] M. Duraiselvam, R. Galun, V. Wesling, B.L. Mordike, R. Reiter, J. Oligmüller, Cavitation erosion resistance of AISI 420 martensitic stainless steel laser-clad with nickel aluminide intermetallic composites and matrix composites with TiC reinforcement, Surf. Coat. Technol. 201 (2006) 1289–1295, https://doi.org/10.1016/j.surfcoat.2006.01.054.

[59] D. Mutaşcu, I. Mitelea, I. Bordeaşu, D. Buzdugan, F. Franţ, Cavitation resistant layers from stellite alloy deposited by TIG welding on duplex stainless steel, in: Proceedings of the 28th International Conference on Metallurgy and Materials, 2019, pp. 776–780. Brno, Czech Republic.

[60] Z. Wang, X. Zhang, J. Cheng, J. Lin, Z. Zhou, Cavitation erosion resistance of Fe-based amorphous/nanocrystal coatings prepared by High-Velocity Arc Spraying, J. Therm. Spray Technol. 23 (2014) 742–749, https://doi.org/10.1007/s11666-014-0074-5.

[61] J. Lin, Z. Wang, J. Cheng, M. Kang, X. Fu, S. Hong, Effect of initial surface roughness on cavitation erosion resistance of arc-sprayed Fe-based amorphous/nanocrystalline coatings, Coatings 7 (2017) 200, https://doi.org/10.3390/coatings7110200.

[62] M.A. Meyers, K.K. Chawla, Mechanical Behavior of Materials, second ed., Cambridge University Press, Cambridge, 2009.

[63] D. Raabe, Z. Li, D. Ponge, Metastability alloy design, MRS Bull. 44 (2019) 266–272, https://doi.org/10.1557/mrs.2019.72.

[64] J.C. Li, X. Lü, Q. Jiang, Composition design of iron-base shape memory alloys, J. Mater. Sci. Lett. 18 (1999) 857–858, https://doi.org/10.1023/A:1006692025752.

[65] H. Otsuka, H. Yamada, T. Maruyama, H. Tanahashl, S. Matsuda, M. Murakami, Effect of aloying additions on Fe-Mn-Si shape memory alloys, ISIJ Int. 30 (1990) 674–679, https://doi.org/10.2355/isijinternational.30.674.

[66] J.H. Kim, K.S. Na, G.G. Kim, J.Y. Oh, C.S. Yoon, S.J. Kim, The effects of Mn and B on the cavitation erosion resistance of austenitic Fe-base hardfacing alloys, Mater. Sci. Eng. A 477 (2008) 204–207, https://doi.org/10.1016/j.msea.2007.05.025.

[67] A. Jahn, A. Kovalev, A. Weiß, P.R. Scheller, Influence of manganese and nickel on the A' martensite transformation temperatures of high alloyed Cr-Mn-Ni steels, Steel Res. Int. 82 (2011) 1108–1112, https://doi.org/10.1002/srin.201100063.

[68] M.C. Park, K.N. Kim, G.S. Shin, S.J. Kim, Effects of strain induced martensitic transformation on the cavitation erosion resistance and incubation time of Fe–Cr–Ni–C alloys, Wear 274–275 (2012) 28–33, https://doi.org/10.1016/j.wear.2011.08.011.

[69] Y.S. Korobov, H.L. Alwan, M.A. Filippov, N.N. Soboleva, I.A. Alani, S. K. Estemirova, A.V. Makarov, V.A. Sirosh, The effect of martensitic transformation on the cavitation erosion resistance of a TIG-deposited Fe-Cr-C-Al-Ti layer, Surf. Coatings Technol. 421 (2021), 127391, https://doi.org/10.1016/j.surfcoat.2021.127391.

[70] M. Lee, Y. Kim, Y. Oh, Y. Kim, S. Lee, H. Hong, S. Kim, Study on the cavitation erosion behavior of hardfacing alloys for nuclear power industry, Wear 255 (2003) 157–161, https://doi.org/10.1016/S0043-1648(03)00144-3.

[71] G. Frommeyer, U. Brüx, P. Neumann, Supra-ductile and high-strength manganese-TRIP/TWIP steels for high energy absorption purposes, ISIJ Int. 43 (2003) 438–446, https://doi.org/10.2355/isijinternational.43.438.

[72] J.Y. Yun, G.S. Shin, M.C. Park, H.S. Lee, W.S. Kang, S.J. Kim, Effect of strain-induced ε and α'-martensitic transformation on cavitation erosion resistance in austenitic Fe-Cr-C-MnFe-Cr-C-mnti alloys, Wear 338–339 (2015) 379–384, https://doi.org/10.1016/j.wear.2015.04.009.

[73] M.C. Park, K.N. Kim, G.S. Shin, J.Y. Yun, M.H. Shin, S.J. Kim, Effects of Ni and Mn on the cavitation erosion resistance of Fe-Cr-C-Ni/Mn austenitic alloys, Tribol. Lett. 52 (2013) 477–484, https://doi.org/10.1007/s11249-013-0231-x.

[74] S. Allain, J.-P. Chateau, O. Bouaziz, S. Migot, N. Guelton, Correlations between the calculated stacking fault energy and the plasticity mechanisms in Fe–Mn–C alloys, Mater. Sci. Eng. A 387–389 (2004) 158–162, https://doi.org/10.1016/j.msea.2004.01.059.

[75] D. Lang, Q. Li, X. Huang, W. Huang, Stacking Fault energy and Fcc→hcp transformation driving force in Fe-Mn-C-Cr-Si high manganese steels and experimental investigation, Mater. Res. Express 8 (2021), 086507, https://doi.org/10.1088/2053-1591/ac1c34.

[76] V.M. Blinov, I.O. Bannykh, E.I. Lukin, O.A. Bannykh, E.V. Blinov, O. P. Chernogorova, M.A. Samoilova, Effect of substitutional alloying elements on the stacking fault energy in austenitic steels, Russ. Metall. 2021 (2021) 1325–1332, https://doi.org/10.1134/S0036029521100086.

[77] M.A. Filippov, B.A. Kulishenko, E.V. Val'kov, Wear resistance of facing alloy with metastable austenite, Met. Sci. Heat Treat. 47 (2005) 6–8, https://doi.org/10.1007/s11041-005-0021-7.

[78] G.S. Shin, J.Y. Yun, M.C. Park, S.J. Kim, Effect of mechanical properties on cavitation erosion resistance in γ → A′ phase transformable Fe–Cr–C–Mn alloys, Tribol. Lett. 57 (2015) 25, https://doi.org/10.1007/s11249-015-0468-7.

[79] J.R. Cruz, S.L. Henke, A.G.M.M. Pukasiewicz, A.S.C.M. D'Oliveira, A.S.C. M. D'Oliveira, The effect of boron on cavitation resistance of FeCrMnSiB austenitic stainless steels, Wear 436–437 (2019), 203041, https://doi.org/10.1016/j.wear.2019.203041.

[80] L. Ma, T. Jia, G. Li, J. Hu, J.A. Jimenez, X. Gao, Mechanical properties enhancement of a novel medium Mn-TRIP/TWIP assisted steel by dispersion of M2B-type borides particles, Mater. Sci. Eng. A (2020) 784, https://doi.org/10.1016/j.msea.2020.139333.

[81] P. Ding, X. Liu, J. Liu, J. Li, H. Li, H. Zhao, J. Duan, Y. Jiao, Study on the properties of FeCrNi/CBN composite coating with high Velocity Arc Spraying, Arab. J. Chem. 11 (2018) 935–941, https://doi.org/10.1016/j.arabjc.2018.02.006.

[82] A.I. Gusev, A.A. Usol'tsev, N.A. Kozyrev, N.V. Kibko, L.P. Bashchenko, Flux-cored wire for the surfacing of parts subject to wear, Steel Transl. 48 (2018) 724–731, https://doi.org/10.3103/S0967091218110037.

[83] L. Li, C. Gui, Dissolving behavior of tungsten carbide in surface welded using flux-cored wire, Procedia Eng. 27 (2012) 823–827, https://doi.org/10.1016/j.proeng.2011.12.526.

[84] K. Yury, M. Filippov, A. Makarov, I. Malygina, N. Soboleva, D. Fantozzi, M. Andrea, H. Koivuluoto, P. Vuoristo, Arc-sprayed Fe-based coatings from coredwires for wear and corrosion protection in power engineering, Coatings 8 (2018) 1–15, https://doi.org/10.3390/coatings8020071.

[85] J. Lin, Z. Wang, P. Lin, J. Cheng, X. Zhang, S. Hong, Microstructure and cavitation erosion behavior of FeNiCrBSiNbW coating prepared by twin wires Arc Spraying process, Surf. Coatings Technol. 240 (2014) 432–436, https://doi.org/10.1016/j.surfcoat.2013.12.071.

[86] W. Guo, J. Zhang, Y. Wu, S. Hong, Y. Qin, Fabrication and characterization of Fe-based amorphous coatings prepared by High-Velocity Arc Spraying, Mater. Des. 78 (2015) 118–124, https://doi.org/10.1016/j.matdes.2015.04.027.

[87] R.F. Vaz, G.B. Sucharski, A. Chicoski, I.B.A.F. Siqueira, R. Tristante, A.G. M. Pukasiewicz, Comparison of FeMnCrSi cavitation resistance coatings deposited by twin-wire electric arc and high-velocity oxy-fuel processes, J. Therm. Spray Technol. 30 (2021) 754–771, https://doi.org/10.1007/s11666-020-01145-z.

[88] R.F. Vaz, A.G.M. Pukasiewicz, H.D.C. Fals, L.A. Lourençato, R.S.C. Paredes, Study of particle properties of different steels sprayed by arc spray process, Coatings 10 (2020) 417, https://doi.org/10.3390/coatings10040417.

[89] J. Wang, Y. Wang, J. Liu, L. Zhang, L. Gao, G. Zheng, H. Shen, J. Sun, Microstructure and flight behaviors of droplet and its solidification in twin-wire arc sprayed Ni-Al composite coatings, Mater. Res. 21 (2018) 1–10, https://doi.org/10.1590/1980-5373-mr-2017-0394.

[90] H. Pokhmurska, M. Student, G. Paczkowski, M. Holovchuk, H. Chumalo, V. Hvozdetskyi, S. Schuberth, Influence of diameter of the cored wires on abrasive wear resistance of arc sprayed coatings, IOP Conf. Ser. Mater. Sci. Eng. 1147 (2021), 012033, https://doi.org/10.1088/1757-899X/1147/1/012033.

[91] Z. Snow, Metal powder production and powder size and shape distribution, in: D. Bourell, W. Frazier, H. Kuhn, M. Seifi (Eds.), Additive Manufacturing Processes, ASM International: Materials Park, vol. 24, Additi, 2020, pp. 167–171.

[92] K. Kassym, A. Perveen, Atomization processes of metal powders for 3D printing, Mater. Today Proc. 26 (2020) 1727–1733, https://doi.org/10.1016/j.matpr.2020.02.364.

[93] J.J. Dunkley, Metal powder atomisation methods for modern manufacturing, Johnson Matthey Technol. Rev. 63 (2019) 226–232, https://doi.org/10.1595/205651319X15583434137356.

[94] D. Bond, S.F. Becker, A.S.C.M. D'Oliveira, Influência Da Corrente e Granulometria Do Material de Adição Nos Revestimentos Processados Por PTA, Soldag. Inspeção 16 (2011) 53–61, https://doi.org/10.1590/S0104-92242011000100007.

[95] R.F. Vaz, A. Silvello, J. Sanchez, V. Albaladejo, I.G.G. Cano, The influence of the powder characteristics on 316L stainless steel coatings sprayed by cold gas spray, Coatings 11 (2021) 168, https://doi.org/10.3390/coatings11020168.

[96] M. Jeandin, G. Rolland, L.L. Descurninges, M.H. Berger, Which powders for cold spray? Surf. Eng. 30 (2014) 291–298, https://doi.org/10.1179/1743294414Y.0000000253.

[97] S. Wirojanupatump, P. Shipway, D. McCartney, The influence of HVOF powder feedstock characteristics on the abrasive wear behaviour of CrxCy–NiCr coatings, Wear 249 (2001) 829–837, https://doi.org/10.1016/S0043-1648(01)00821-3.

[98] K. Bobzin, M. Öte, M.A. Knoch, J. Sommer, Influence of powder size on the corrosion and wear behavior of HVAF-sprayed Fe-based coatings, J. Therm. Spray Technol. 28 (2019) 63–75, https://doi.org/10.1007/s11666-018-0819-7.

[99] A.G.M. Pukasiewicz, A.R. Capra, R.S.C. Paredes, Cavitation erosion mechanism in Fe-Mn-Cr-Si-Ni arc thermally sprayed coatings, in: B.R. Marple, A. Agarwal, M. M. Hyland, Y.C. Lau, C.J. Li, R.S. Lima, A. McDonald (Eds.), Proceedings of the ITSC 2011 - Proceedings of the International Thermal Spray Conference, Springer, Hamburg, Germany, 2011.

[100] A.G.M. Pukasiewicz, A.R. Capra, R.S.C. Paredes, A.S.C. Oliveira, Development of arc thermally sprayed Fe-Mn-Cr-Si coatings against cavitation erosion, in: B. R. Marple, A. Agarwal, M.M. Hyland, Y.C. Lau, C.J. Li, R.S. Lima, A. McDonald (Eds.), Proceedings of the ITSC 2011 - Proceedings of the International Thermal Spray Conference Conference Proceedings, ASM International, Hamburg, Germany, 2011.

[101] A.P. Newbery, P.S. Grant, Oxidation during electric arc spray forming of steel, J. Mater. Process. Technol. 178 (2006) 259–269, https://doi.org/10.1016/j.jmatprotec.2006.03.176.

[102] S. Tailor, N. Vashishtha, A. Modi, S.C. Modi, Oxidation control in arc-sprayed SS420 coating, Surf. Eng. 37 (2021) 581–589, https://doi.org/10.1080/02670844.2020.1840696.

[103] Y. Li, D.S. Martín, J. Wang, C. Wang, W. Xu, A review of the thermal stability of metastable austenite in steels: martensite Formation, J. Mater. Sci. Technol. 91 (2021) 200–214, https://doi.org/10.1016/j.jmst.2021.03.020.

[104] P. Maitrepierre, D. Thivellier, R. Tricot, Influence of boron on the decomposition of austenite in low carbon alloyed steels, Metall. Trans. A 6 (1975) 287–301, https://doi.org/10.1007/BF02667283.

[105] M.I. Razikov, V.I. Shumyakov, V.Ya. Dubskikh, inventors; S. M. Kirov Urals Polytechnic Institute, assignee. Cored wire. USSR patent 280212. 1970 Nov 24.

[106] G.B. Sucharski, A.GeM. Pukasiewicz, R.F. Váz, R.S.C. Paredes, Optimization of the deposition parameters of HVOF FeMnCrSi+Ni+B thermally sprayed coatings, Soldag. Inspeção 20 (2015) 238–252, https://doi.org/10.1590/0104-9224/SI2002.11.

[107] L.L. Silveira, A.G.M. Pukasiewicz, D.J.M. de Aguiar, A.J. Zara, S. Björklund, Study of the corrosion and cavitation resistance of HVOF and HVAF FeCrMnSiNi and FeCrMnSiB coatings, Surf. Coatings Technol. 374 (2019) 910–922, https://doi.org/10.1016/j.surfcoat.2019.06.076.

[108] A.G.M. Pukasiewicz, H.E. de Boer, G.B. Sucharski, R.F. Vaz, L.A.J. Procopiak, The influence of HVOF spraying parameters on the microstructure, residual stress and cavitation resistance of FeMnCrSi coatings, Surf. Coatings Technol. 327 (2017) 158–166, https://doi.org/10.1016/j.surfcoat.2017.07.073.

[109] J.R. da Cruz, S.L. Henke, A.S.C.M. D'Oliveira, Effect of cold work on cavitation resistance of an austenitic stainless steel coating, Mater. Res. 19 (2016) 1033–1041, https://doi.org/10.1590/1980-5373-MR-2015-0442.

[110] T.S. Sidhu, S. Prakash, R.D. Agrawal, Studies on the properties of high-velocity oxy-fuel thermal spray coatings for higher temperature applications, Mater. Sci. 41 (2005) 805–823, https://doi.org/10.1007/s11003-006-0047-z.

[111] M. Kelkar, J. Heberlein, Wire-Arc spray modeling, Plasma Chem. Plasma Process. 22 (2002) 1–25, https://doi.org/10.1023/A:1012924714157.

[112] G.D. Lunn, M.A. Riley, D.G. McCartney, A study of wire breakup and in-flight particle behavior during wire Flame spraying of aluminum, J. Therm. Spray Technol. 26 (2017) 1947–1958, https://doi.org/10.1007/s11666-017-0639-1.

[113] I. Gedzevicius, A.V. Valiulis, Analysis of wire Arc Spraying process variables on coatings properties, J. Mater. Process. Technol. 175 (2006) 206–211, https://doi.org/10.1016/j.jmatprotec.2005.04.019.

[114] L.L. Silveira, G.B. Sucharski, A.G.M. Pukasiewicz, R.S.C. Paredes, Influence of particle size distribution on the morphology and cavitation resistance of high-velocity oxygen fuel coatings, J. Therm. Spray Technol. 27 (2018) 695–709, https://doi.org/10.1007/s11666-018-0708-0.

[115] A. Mohankumar, T. Duraisamy, D. Sampathkumar, S. Ranganathan, G. Balachandran, M. Kaliyamoorthy, M. Mariappan, L. Mulugeta, Optimization of cold spray process inputs to minimize porosity and maximize hardness of metal matrix composite coatings on AZ31B magnesium alloy, J. Nanomater. (2022) 1–17, https://doi.org/10.1155/2022/7900150, 2022.

[116] V.K. Champagne, D.J. Helfritch, M.D. Trexler, B.M. Gabriel, The effect of cold spray impact velocity on deposit hardness, Model. Simulat. Mater. Sci. Eng. 18 (2010), 065011, https://doi.org/10.1088/0965-0393/18/6/065011.

[117] M. Vishnoi, P. Kumar, Q. Murtaza, A review on coating for hydro-turbine application by HVOF process, in: I. Singh, P.K. Bajpai, K. Panwar (Eds.), Advances in Materials Engineering and Manufacturing Processes, Springer, Singapore, 2020, pp. 79–103.

[118] G. Hou, X. Zhao, H. Zhou, J. Lu, Y. An, J. Chen, J. Yang, Cavitation erosion of several oxy-fuel sprayed coatings tested in deionized water and artificial seawater, Wear 311 (2014) 81–92, https://doi.org/10.1016/j.wear.2013.12.026.

[119] M. Grujicic, C.L. Zhao, W.S. DeRosset, D. Helfritch, Adiabatic shear instability based mechanism for particles/substrate bonding in the cold-gas dynamic-spray process, Mater. Des. 25 (2004) 681–688, https://doi.org/10.1016/j.matdes.2004.03.008.

[120] R.F. Vaz, A. Garfias, V. Albaladejo, J. Sanchez, I.G. Cano, A review of advances in cold spray additive manufacturing, Coatings 13 (2023) 267, https://doi.org/10.3390/coatings13020267.

[121] C.-J. Li, Y.-Y. Wang, Effect of particle state on the adhesive strength of HVOF sprayed metallic coating, J. Therm. Spray Technol. 11 (2002) 523–529, https://doi.org/10.1361/105996302770348655.

[122] D.E. Crawmer, Coating structures, properties, and materials, in: J.R. Davis (Ed.), Handbook of Thermal Spray Technology, ASM Thermal Spray Society, Materials Park, OH, USA, 2004, pp. 47–53.

[123] J. Matejicek, S. Sampath, Intrinsic residual stresses in single splats produced by thermal spray processes, Acta Mater. 49 (2001) 1993–1999, https://doi.org/10.1016/S1359-6454(01)00099-4.

[124] T.W. Clyne, S.C. Gill, Residual stresses in thermal spray coatings and their effect on interfacial adhesion: a review of recent work, J. Therm. Spray Technol. 5 (1996) 401–418, https://doi.org/10.1007/BF02645271.

[125] R. Ali, M. Sebastiani, E. Bemporad, Influence of Ti–TiN multilayer PVD-coatings design on residual stresses and adhesion, Mater. Des. 75 (2015) 47–56, https://doi.org/10.1016/j.matdes.2015.03.007.

[126] V. Teixeira, Residual stress and cracking in thin PVD coatings, Vacuum 64 (2002) 393–399, https://doi.org/10.1016/S0042-207X(01)00327-X.

[127] C. Lee, H. Park, J. Yoo, C. Lee, W. Woo, S. Park, Residual stress and crack initiation in laser clad composite layer with Co-based alloy and WC + NiCr, Appl. Surf. Sci. 345 (2015) 286–294, https://doi.org/10.1016/j.apsusc.2015.03.168.

[128] ASTM *G32-03 - Standard Test Method for Cavitation Erosion Using Vibratory Apparatus*, ASTM International, West Conshohocken, PA, USA, 2003.

[129] ASTM *G134-95 - Standard Test Method for Erosion of Solid Materials by Cavitating Liquid Jet*, ASTM International, West Conshohocken, PA, USA, 2010.
[130] A.R. Mayer, K. Bertuol, I.B.A.F. Siqueira, A. Chicoski, R.F. Váz, M.J. de Sousa, A. G.M.M. Pukasiewicz, Evaluation of cavitation/corrosion synergy of the Cr3C2-25NiCr coating deposited by HVOF process, Ultrason. Sonochem. 69 (2020) 1–9, https://doi.org/10.1016/j.ultsonch.2020.105271.
[131] L.A. Luiz, J. de Andrade, C.M. Pesqueira, I.B.A.F. Siqueira, G.B. Sucharski, M.J. de Sousa, Corrosion behavior and galvanic corrosion resistance of WC and Cr3C2 cermet coatings in madeira river water, J. Therm. Spray Technol. 30 (2021) 205–221, https://doi.org/10.1007/s11666-021-01152-8.
[132] S. Sinha, S.S. Nene, M. Frank, K. Liu, P. Agrawal, R.S. Mishra, On the evolving nature of c/a ratio in a hexagonal close-packed epsilon martensite phase in transformative high entropy alloys, Sci. Rep. 9 (2019), 13185, https://doi.org/10.1038/s41598-019-49904-5.
[133] I.A. Yakubtsov, A. Ariapour, D.D. Perovic, Effect of nitrogen on stacking fault energy of f.c.c. Iron-based alloys, Acta Mater. 47 (1999) 1271–1279, https://doi.org/10.1016/S1359-6454(98)00419-4.
[134] ASTM *G65-00 - Standard Test Method for Measuring Abrasion*, Using the Dry Sand Rubber Wheel Apparatus, ASTM International, West Conshohocken, PA, USA, 2000.
[135] M.K. Linnenluecke, M. Marrone, A.K. Singh, Conducting systematic literature reviews and bibliometric analyses, Aust. J. Manag. 45 (2020) 175–194, https://doi.org/10.1177/0312896219877678.
[136] N. Donthu, S. Kumar, D. Mukherjee, N. Pandey, W.M. Lim, How to conduct a bibliometric analysis: an overview and guidelines, J. Bus. Res. 133 (2021) 285–296, https://doi.org/10.1016/j.jbusres.2021.04.070.
[137] T. Zhao, S. Zhang, Z.Y. Wang, C.H. Zhang, Y. Liu, C.L. Wu, Modulating heat input to optimize corrosion and synergistic cavitation erosion-corrosion behavior of Ni201 cladding layer by cold metal transfer, Surf. Coatings Technol. 443 (2022), 128595, https://doi.org/10.1016/j.surfcoat.2022.128595.
[138] T.B. Thiagarajan, S. Ponnusamy, Effect of cladding of stellite-6 filler wire on the surface of SS316L alloy through cold Metal Arc transfer process, J. Met. Mater. Miner. 31 (2021) 70–84, https://doi.org/10.14456/jmmm.2021.41.
[139] P. Kołodziejczak, M. Bober, T. Chmielewski, Wear resistance comparison research of high-alloy protective coatings for power industry prepared by means of CMT cladding, Appl. Sci. 12 (2022) 4568, https://doi.org/10.3390/app12094568.
[140] G. Lorenzin, G. Rutili, The innovative use of low heat input in welding: experiences on 'cladding' and brazing using the CMT process, Weld. Int. 23 (2009) 622–632, https://doi.org/10.1080/09507110802543252.
[141] C. Munro, J. Chen, Direct comparison of cold metal transfer to laser hot-wire cladding for AISI 4340 structural steel repair, Sci. Technol. Weld. Join. 26 (2021) 11–19, https://doi.org/10.1080/13621718.2020.1824450.
[142] S. Cao, J. Liang, J. Zhou, Evolution in microstructure features and properties of Mo-containing Fe-Cr-Ni-B-Si composite coatings by laser cladding, Mater. Char. 188 (2022), 111926, https://doi.org/10.1016/j.matchar.2022.111926.
[143] C. Liu, P. Xu, C. Pang, G. Zha, Z. Ouyang, J. Chen, Phase transformation in Fe–Mn–Si SMA/WC composite coating developed by laser cladding, Mater. Chem. Phys. 267 (2021), 124595, https://doi.org/10.1016/j.matchemphys.2021.124595.
[144] J. Tian, P. Xu, Q. Liu, Effects of stress-induced solid phase transformations on residual stress in laser cladding a Fe-Mn-Si-Cr-Ni alloy coating, Mater. Des. 193 (2020), 108824, https://doi.org/10.1016/j.matdes.2020.108824.
[145] J. Tian, P. Xu, J. Chen, Q. Liu, Microstructure and phase transformation behaviour of a Fe/Mn/Si/Cr/Ni alloy coating by laser cladding, Opt Laser. Eng. 122 (2019) 97–104, https://doi.org/10.1016/j.optlaseng.2019.06.003.
[146] D. Bu, H. Peng, Y. Wen, N. Li, Influence of ageing on wear resistance of an Fe–Mn–Si–Cr–Ni–Ti–C shape memory alloy, Mater. Des. 32 (2011) 2969–2973, https://doi.org/10.1016/j.matdes.2011.01.032.
[147] S. Jeong, Y. Lee, G. Park, B. Kim, J. Moon, S.-J. Park, C. Lee, Phase transformation and the mechanical characteristics of heat-affected zones in austenitic Fe–Mn–Al–Cr–C lightweight steel during post-weld heat treatment, Mater. Char. 177 (2021), 111150, https://doi.org/10.1016/j.matchar.2021.111150.
[148] S. Choi, E. Choi, W.J. Kim, Austenite grain size effect on recovery stress and recovery strain of Fe-Mn-Si-Cr-Ni-0.01C alloy severely plastically deformed by differential speed rolling, Mater. Char. 175 (2021), 111097, https://doi.org/10.1016/j.matchar.2021.111097.
[149] A.S.C. d'Oliveira, R. Vilar, C. Feder, High temperature behaviour of plasma Transferred Arc and laser Co-based alloy coatings, Appl. Surf. Sci. 201 (2002) 154–160, https://doi.org/10.1016/S0169-4332(02)00621-9.
[150] A.G.M. Pukasiewicz, P.R.C. Alcover, A.R. Capra, R.S.C. Paredes, Influence of plasma remelting on the microstructure and cavitation resistance of arc-sprayed Fe-Mn-Cr-Si alloy, J. Therm. Spray Technol. 23 (2014) 51–59, https://doi.org/10.1007/s11666-013-0001-1.
[151] C.V. Roa, J.A. Valdes, F. Larrahondo, S.A. Rodríguez, J.J. Coronado, Comparison of the resistance to cavitation erosion and slurry erosion of four kinds of surface modification on 13-4 Ca6NM hydro-machinery steel, J. Mater. Eng. Perform. 30 (2021) 7195–7212, https://doi.org/10.1007/s11665-021-05908-9.
[152] G. Park, G. Bae, K. Moon, C. Lee, Effect of plasma nitriding and nitrocarburizing on HVOF-sprayed stainless steel coatings, J. Therm. Spray Technol. 22 (2013) 1366–1373, https://doi.org/10.1007/s11666-013-0035-4.